R. & M. No. 2321
(10,462)
A.R.C. Technical Report

MINISTRY OF SUPPLY

AERONAUTICAL RESEARCH COUNCIL
REPORTS AND MEMORANDA

Investigation of the Flow past Finite Wedges of 20 deg. and 40 deg. Apex Angle at Subsonic and Supersonic Speeds, using a Mach-Zehnder Interferometer

By
D. C. PACK

With Appendix : Sensitivity and Accuracy of the Interference Method applied to Pressure Measurements
By
E. GROTH

LONDON : HIS MAJESTY'S STATIONERY OFFICE
1949
SIX SHILLINGS NET

Investigation of the Flow past Finite Wedges of 20 deg. and 40 deg. Apex Angle at Subsonic and Supersonic Speeds, using a Mach-Zehnder Interferometer

By

D. C. PACK

With Appendix: Sensitivity and Accuracy of the Interference Method applied to Pressure Measurements

By

E. GROTH

COMMUNICATED BY THE PRINCIPAL DIRECTOR OF SCIENTIFIC RESEARCH (AIR), MINISTRY OF SUPPLY

Reports and Memoranda No. 2321

May, 1946*

Summary.—An investigation has been made in the high-speed wind tunnel A 7 of the Luftfahrtforschungsanstalt, Brunswick, of the flow past finite wedges of 20 deg. and 40 deg. apex angle at both subsonic and supersonic speeds, the Mach numbers lying between 0·6 and 0·85 on the one hand, and between 1·4 and 2·8 on the other. The pressure distributions on the models have been evaluated from photographs of density contours obtained by the use of a Mach-Zehnder interferometer. The interferometer technique is briefly described, and also the method of evaluation of the photographs.

The results are discussed in detail, and are compared with the theoretical predictions of Maccoll and Codd. A selection of photographs, and a number of diagrams showing the pressure distribution, are included.

In the Appendix, the sensitivity and accuracy of the interference method applied to pressure measurements are discussed. It is shown that requirements for both, in the particular case of the A 7 tunnel, are satisfied in a range of Mach numbers between 0·5 and 3·0.

1. *Introduction.*—In February and March, 1946, in the small high-speed wind tunnel A 7 of the Luftfahrtforschungsanstalt, Brunswick, a series of tests was carried out on the two-dimensional flow past two finite wedges of 20 deg. and 40 deg. apex angle, respectively. The range of Mach numbers included both subsonic and supersonic velocities.

In addition to the usual static tubes for pressure measurements, the flow was examined by means of a Mach-Zehnder interferometer, which enabled photographs to be taken of the density configuration. Using the interferometry technique, it is possible to study the density and pressure distributions, not only at the surface of the profile, but over the whole field of flow.

The work described here was carried out under the author's direction by a team headed by Dipl.-Ing. W. Richter, who set up and operated the interferometer, and by Dr.-Phil. E. Groth, who has developed the method of evaluation of interference photographs[1, 2]. The main formulae for the evaluation are recounted for the sake of convenience of reference, and a brief

* Ministry of Supply Armament Research Department Theoretical Research Report No. 4/46 received 24th March, 1947.

description of the optical method is included. In an appendix to the report, Dr. Groth discusses the sensitivity and accuracy of the interferometer technique, showing that general requirements for both, with a wind tunnel of the size of A 7 and with the given apparatus, can be satisfied simultaneously in a range of Mach numbers from 0·5 to 3·0 approximately.

A selection of photographs is given of the flow at both subsonic and supersonic velocities past the two models, showing lines of constant density or fringe displacements, according to the choice of interferometer set-up. The density contours are more generally used, since they simplify the analysis, and at the same time, they enable a quick appreciation of the type of flow to be made ; in particular, they provide a beautiful illustration of the radial character of the well-known Meyer expansion in supersonic flow round a corner (see, for example, Fig. 15). For comparison with the interference photographs, some shadowgraph pictures, showing shock waves and steep density gradients in supersonic flow, have been included.

Calculations of the variation of the pressure coefficient over the surface of the model are presented graphically, as also is the distribution of Mach number in the flow for a few cases, in order to show the position of the sonic line and the extent of the region of supersonic flow where the flow is mixed subsonic and supersonic.

Comparisons are made between the results of these experiments and the calculations of Maccoll and Codd.[3] There is some deviation of a quantitative nature, which can probably be explained by the fact that it was not possible to dry the air in the wind tunnel for the purpose of these experiments, but the qualitative predictions are amply supported by the results. For subsonic speeds of the incident air the density contours spring at right-angles from the surface of a wedge, and the sonic line begins at or very close to the shoulder. The fundamental assumptions upon which Maccoll and Codd based their formula for the resistance of a wedge in the trans-sonic region of velocities (Mach number M_1 of incident flow between about 0·7 and 1·5) seem to be valid, judging by the comparison of the distribution of p/p_1 for $M_1 = 1{\cdot}4$ and for a subsonic range from $M_1 = 0{\cdot}7$ to 0·8. The similarity of the distributions over the wedge for $M_1 = 0{\cdot}8$ and $M_1 = 1{\cdot}4$ for the 40 deg. wedge, is to be noted (Fig. 14).

2. *Description of the Tunnel Arrangement.*—The wind tunnel A 7 is of return circuit, closed-jet type, the air being circulated in the present tests by a 4-stage centrifugal compressor powered by a 1,500 r.p.m., 1,000 kW. Siemens motor. The air on the high pressure side of the compressor passes through a water cooler before entering the settling chamber via a honeycomb. The working section for subsonic tests is 250 mm. square ; for supersonic tests the span remains unaltered, but the height depends upon the shape of the nozzle used to produce the supersonic flow, and the values for the series of experiments described in this report are given in Fig. 25.

For the measurement of pressures a multimanometer was used. Static pressure, total pressure and temperature measurements were made for the settling chamber. The velocity of the air in the settling chamber is in all cases negligible compared with that in the working section, and static and dynamic pressure measurements there may be considered equal, and denoted by p_0, the total head. Pressures in and behind the tunnel working section were recorded by static tubes ; in subsonic tests these were on the upper and lower faces of the tunnel, and in supersonic tests on the sides. The static pressure p_1 at the beginning of the working section gives the Mach number of the flow at once if the total head is known, provided that conditions at the point of measurement of p_1 are not influenced by conditions downstream, since by combination of the adiabatic relationship,

$$p/\rho^\gamma = \text{const.}, \quad \ldots \quad \ldots \quad \ldots \quad \ldots \quad \ldots \quad \ldots \quad \ldots \quad (1)$$

(where γ is the ratio of specific heats, put equal to 1·405 for air, and ρ denotes density) with Bernoulli's equation :

$$\tfrac{1}{2}w^2 + \frac{\gamma}{\gamma - 1} p/\rho = \frac{\gamma}{\gamma - 1} p_0/\rho_0 \quad \ldots \quad \ldots \quad \ldots \quad \ldots \quad \ldots \quad \ldots \quad (2)$$

in which w = resultant velocity, and the suffix zero (as always in this report) refers to conditions in the settling chamber, we may derive at once

$$\frac{\gamma - 1}{2} M_1^2 + 1 = \left\{\frac{p_0}{p_1}\right\}^{(\gamma - 1)/\gamma} \quad .. \quad .. \quad .. \quad .. \quad .. \quad .. \quad (3)$$

The suffix unity will always be used for conditions in the free stream ; M represents the Mach number, i.e., the ratio of the velocity at any point to the local velocity of sound.

3. *Optical Arrangement.*—3.1. For the optical investigation of the flow in the wind tunnel a Mach-Zehnder interferometer was used. This apparatus has been described in a number of reports (see, for example, Ref. 6). It consists of four mirrors, two of which are half-silvered to permit passage of light. The light from the source S is divided at mirror 1 and is re-united at mirror 4 (Fig. 1 is a schematic drawing). The light rays from mirror 3 pass through the tunnel working section before reaching mirror 4. In the path between mirrors 1 and 2 a cylinder C with glass windows is placed, in order to correct the length of the optical path of this arm of the interferometer relative to the other arm which passes through the side windows of the wind tunnel. The mirrors 1 and 4 are free to turn about two perpendicular axes in their planes. The mirrors 2 and 3 are rigidly fixed, parallel to one another and at 45 deg. to the " sides ".

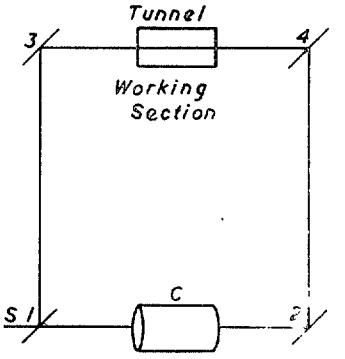

FIG. 1.

In all that follows we assume that the light entering the interferometer from the source S is in the form of a parallel beam.

3.2. *Zero Interference.*—When not strictly monochromatic light is used, a very careful adjustment of the apparatus is required in order to find the position of zero interference (" Nullinterferens " of the German literature). This is the position in which the optical paths in the two arms of the interferometer between mirrors 1 and 4 are exactly equal. All wavelengths then arrive at 4 in phase, and distinguishable fringes can be produced. Failing the zero interference, the difference of the fringe widths corresponding to different wavelengths in the light used (see below), coupled with the initial phase difference, causes the fringes to be obscured on superposition. The amount of error allowable in practice, where a sufficient number of sharp fringes must be obtained, is only a few thousandths of a millimetre.

3.3. *Initial Configurations.*—We assume that, for non-chromatic light, the " zero inferference " has been found and that the dominant wavelength is known for the given light.

If all mirrors are initially parallel at 45 deg. to the incoming light, no interference fringes are to be seen. When density changes occur in the wind tunnel however, involving density gradients, interference fringes begin to appear, each fringe representing a change in density from the initial value, the magnitude of the density change being constant along its length, one new fringe appearing for each successive wavelength difference in the optical paths. For this reason we shall call this initial set-up the " density contour configuration ", and the fringes " density contour fringes " or " contour interference fringes ". The German title for this arrangement is " Mittelfigur ".

If we turn the mirror 1 we obtain fringes initially, the location being virtually at mirror 4. By turning both mirrors 1 and 4, the plane of the fringes can be brought to the mid-plane of the span of the model (only a plane of fringes exists if we do not have a point source of light). In this case the fringes in the middle of the tunnel can be photographed in focus with the profile under investigation. The arrangement by which two mirrors are turned to produce fringes initially—fringes which suffer displacement when density changes occur in the tunnel—we shall call the " displacement configuration ", and the fringes we shall call " displacement interference fringes ". The German name for the configuration is " Interferenz ". The suggested English titles for the two configurations will, it is hoped, lead to a clearer understanding than the original German titles, which have not been very satisfactory choices.

In the density contour configuration the question of focussing the fringes does not arise ; and even if there is a slight departure from parallelism in the light from the source, it is easy to show that the effect on definition will always be least in the centre of the tunnel, so that optically, as well as aerodynamically, the best results are to be expected by focussing the camera on the mid-plane of the span, and, if one wishes to use the displacement configuration, by focussing the interference fringes on to the same plane.

3.4. *Optical Formulae.*—Setting off from the displacement configuration, let b be the distance between two consecutive initial fringes, and y the displacement of a fringe corresponding to a density ρ. Let L be the length of the span of the tunnel (i.e., the length of the light path in which the density may be disturbed), n the refractive index at the point with density ρ, pressure p and temperature T. Let λ_v be the wavelength of the parallel light in vacuo (λ_v must in practice be taken as the dominant wavelength, if the light used is not monochromatic).

First, we have the optical law $\dfrac{n-1}{\rho} = \text{const.}$, ... (4)

Next, we have the relation between displacement and breadth of fringes, which is easily deducible

$$\frac{y}{b} = \frac{n - n_s}{\lambda_v} \cdot L \qquad .. \quad .. \quad .. \quad .. \quad .. \quad .. \quad .. \quad .. \quad (5)$$

referring all displacements to a base point in the flow (of refractive index n_s) at which the pressure (density) is known. Such a point may be obtained by a manometer measurement, and in this way the problem of making absolute measurements outside the tunnel is avoided.

If we set up the density contour configuration, in which no lines are initially to be seen, the value of b is infinite, and in this case the quantity y/b represents the *number* of fringes introduced by the density changes corresponding to the change of refractive index. This arrangement is in general more suitable for study, as it facilitates the evaluation considerably, and also, since each fringe is a density contour, it presents to the eye a more easily interpretable picture of the flow.

3.5. *Compensation of Optical Paths.*—In each arm of the interferometer there is a compensating plate, by means of which fine adjustment can be made to the length of either optical path. Further, in order to allow for the main changes in optical path due to density changes in the working section, the latter may be connected with the cylinder C by means of a pressure hole and tube, so that the cylinder has the same pressure as the working section. At low speeds this implies equal density in C also, but at supersonic speeds, where the difference between the densities given isothermally in the cylinder and adiabatically in the tunnel, for the same pressure, is too great for the correction to be made by means of the compensation plates, it was necessary to remove the connection and fit an evacuation pump to the cylinder instead. By this means, air could be removed from the cylinder by the pump, or let in by a tap, and adjustments of large magnitude were possible.

3.6. *The Optical and Spark Method.*—The methods adopted for photographing the fringes were dictated by the available apparatus and the limited time for completion of the work. The means of producing a parallel beam of light are shown in Fig. 2. The light source was a spark, obtained by the discharge of a 30 kV., 0·5 microfarad condenser across an open-air gap of 8 mm. between two copper spheres of 25 mm. diameter. The duration of the spark was of the order 10^{-6} seconds. The light passed through a lens which focussed it into a red Zeiss filter (RG II), thus eliminating all wavelengths below about 5,700 Å. The transmitted light was constrained into a parallel beam by a parabolic mirror, and then reflected into the interferometer. On the opposite side of the wind tunnel a reflecting mirror was placed at its focal distance from the centre of the tunnel, and this focussed the fringes and profile into the camera. The film used for the photographs was RAF Panchromatic, and the camera was an RAF F.24. The film had a good red absorption, and hence combined with the light transmitted by the red filter to produce good definition of the interference fringes.

4. *Evaluation of Interference Photographs.*—4.1. The method of evaluation of interference photographs has been outlined by Groth[1, 2]. When the flow is two-dimensional, as in the present series of wedge tests, no great difficulty arises. The possible errors from the aerodynamical point of view arise from faults in the velocity distribution across the tunnel, and the effect of the boundary layers at the sides of the tunnel. The flow in these experiments is also symmetrical, subject to any error in the setting of the wedges at zero incidence to the stream. These possible effects have been neglected ; in particular, the boundary layer effect at the side walls is neglected in comparison with the effect of the main flow over the remainder of the span.

Under these circumstances we have the optimum conditions for the use of the interferometer technique, since the state of the air may be considered constant along a light ray during the passage of the ray through the working-section.

The method of evaluation for two-dimensional flow is recounted briefly in the following paragraphs, where we preserve as far as possible the terminology of Durand, *Aerodynamics*, Vol. 3 (Ref. 4).

4.2. *Equations.*—First of all we have the optical equations from the previous section

$$\frac{n-1}{\rho} = \text{const.}, \qquad \ldots\ldots\ldots\ldots\ldots\ldots\ldots\ldots \quad (4)$$

$$\frac{y}{b} = \frac{n-n_1}{\lambda_v} \cdot L \qquad \ldots\ldots\ldots\ldots\ldots\ldots\ldots\ldots \quad (5)$$

where we take the base point (n_s) to be one at which the conditions of the free stream (n_1) are found.

Next we add to our equations the equation of state, and the adiabatic relationship—

$$p = RT\rho \qquad \ldots\ldots\ldots\ldots\ldots\ldots\ldots\ldots \quad (6)$$

$$p/p_1 = (\rho/\rho_1)^\gamma \qquad \ldots\ldots\ldots\ldots\ldots\ldots\ldots\ldots \quad (7)$$

where R is the gas constant, and the other symbols are as already defined. The suffix unity is used to represent the free stream conditions, which are the conditions at the beginning of the working section (provided there is negligible influence from the model), or, in the case of supersonic flow, the conditions upstream of the shock wave.

The pressure ratio may at once be written in the form

$$p/p_1 = (1 + c_s)^\gamma \qquad \ldots\ldots\ldots\ldots\ldots\ldots\ldots\ldots \quad (8)$$

with

$$c_s = \frac{\lambda_v}{L \cdot \underline{\frac{n-1}{\rho}} \cdot \rho_1} \cdot \frac{y}{b} = \frac{\lambda_v}{L \cdot \underline{\frac{n-1}{\rho}} \cdot \rho_0} \cdot \frac{\rho_0}{\rho_1} \cdot \frac{y}{b} \qquad \ldots\ldots\ldots\ldots \quad (9)$$

c_s has been called the " shift coefficient " by Groth[2]. The quantity p/p_1 is the usual ratio for presenting results of supersonic tests, and we use it also in this report for the subsonic tests, for the purpose of comparison.

For very low velocities of flow, the above equation (8) can be linearised to

$$(p/p_1)_{lin} = 1 + \gamma c_s \qquad \ldots\ldots\ldots\ldots\ldots\ldots\ldots\ldots \quad (8a)$$

i.e. $$(\Delta p/p_1)_{lin} = \gamma c_s. \qquad \ldots\ldots\ldots\ldots\ldots\ldots\ldots\ldots \quad (8a) \text{ bis}$$

For high subsonic speeds, by expansion of (8),

$$\left(\frac{\Delta p}{p_1}\right) = \left(\frac{\Delta p}{p_1}\right)_{lin} \left\{ 1 + \frac{\gamma - 1}{2\gamma} \left(\frac{\Delta p}{p_1}\right)_{lin} \right\} \qquad \ldots\ldots\ldots\ldots \quad (8b)$$

The neglected terms in the expansion contribute less than 1 per cent. to the value of $\frac{\Delta p}{p_1}$ if $M_1 < 1$.

For supersonic velocities of flow the equation (8) is used unchanged. For the free stream we see that $c_s = 0$, and for vacuum $c_s = -1$. For a stagnation point

$$c_s = \left\{(1 + \frac{\gamma - 1}{2} M_1^2)^{1/(\gamma-1)} - 1\right\}$$

The shift coefficient is best written in the form $c_s = A \cdot \frac{\rho_0}{\rho_1} \cdot \frac{y}{b}$, where A is constant for given chamber conditions and $\frac{\rho_0}{\rho_1}$ is a known function of M_1 by (3). The equations are further considered in the appendix to this report, where the sensitivity of the interference method and the accuracy of the evaluations are discussed at length.

4.3. *The Effect of a Shock Valve.*—In passing through a straight shock wave the total head of the flow is reduced from p_0 to p_3, say, and we have $K = p_3/p_0 = \rho_3/\rho_0$, a relation following at once from the equation of conservation of energy. K has been called the " diminution factor " (" Drosselfaktor ") by Schubert[5], who has calculated it as a function of $M_1 \cos \alpha$, where M_1 is the Mach number of the flow incident upon the shock wave, and α the angle between the direction of the flow and the normal to the shock wave. The relation is—

$$K = \left\{\frac{\gamma + 1}{2}\right\}^{(\gamma+1)/(\gamma-1)} \left\{\frac{M_1^2 \cos^2 \alpha}{1 + \frac{\gamma - 1}{2} M_1^2 \cos^2 \alpha}\right\}^{\gamma/(\gamma-1)} \left\{\frac{1}{\gamma M_1^2 \cos^2 \alpha - \frac{\gamma - 1}{2}}\right\}^{1/(\gamma-1)}$$

and it is tabulated in the report quoted (Schubert denotes by γ the complement of our angle α). The pressure coefficient for the flow behind a shock wave may be written

$$p'/p_1 = K^{1-\gamma}(1 + c_s)^\gamma \quad .. \quad .. \quad .. \quad .. \quad .. \quad .. \quad .. \quad (10)$$

which differs from (8) only in the factor $K^{1-\gamma}$ multiplying the right-hand side. A dash will always be used to denote conditions behind the shock wave.

Writing $K^{1-\gamma} = 1 + \varepsilon$, we may express the last equation in the alternative form $\frac{p' - p_1}{p_1} = \frac{\Delta p'}{p_1} = (1 + \varepsilon) \frac{\Delta p}{p_1} + \varepsilon$, where $\frac{\Delta p}{p_1}$ is the coefficient calculated from a photograph with neglect of the loss of total head. ε has been plotted in Fig. 26.

4.4. *The Zero Fringe.*—Beginning with the contour configuration, a difference of one wavelength in the optical paths of the interferometer, produced by a density change, will result in the appearance of one fringe, and each successive wavelength difference will produce a new fringe. The field of flow has in all cases been evaluated from density-contour photographs, a process which, from the preceding remarks, requires only the counting of the number of fringes from a standard fringe on which conditions are known. We choose as standard fringe the one for which $\Delta p/p_1$ is zero, the " zero fringe ". It is necessary to determine this fringe.

When a number of manometer readings are available for the pressure along the surface of the model, one of the readings is taken as a base, and the nearest fringe to the corresponding pressure hole is given the appropriate fringe number calculable from the formulae of this section. Hence, knowing the direction of the pressure gradient, we may count back to the zero fringe and number all the fringes in a photograph.

There is a possibility of error in this procedure, dependent upon the reliability of the manometer readings ; it is necessary to choose the pressure tube of reference in some part of the field where there are neither shock waves nor rapid fluctuations.

4.5. *Numerical Values.*—For the evaluations the values of the fixed quantities occurring in the equations were taken as follows :—

$$\lambda_v = 6200\text{Å}$$

$$L = 252 \text{ mm.}$$

$$\frac{n-1}{\rho} = 0{\cdot}00222 \text{ (metres)}^4 \text{ kg}^{-1} \text{ sec}^{-2}$$

$$\gamma = 1{\cdot}405$$

$$A = 0{\cdot}0132\rho_0$$

ρ_0 is to be measured in (kg)/(metres)^4 sec^{-2}.

5. *Description of Models : Mounting.*—The models used were wedges of steel, of 20 deg. and 40 deg. apex angle respectively. Each wedge was 240 mm. long and 8 mm. thick. The length of the sloping edge was 22 mm. for the 20 deg. wedge and 11·7 mm. for the 40 deg. wedge. The tail of each model was tapered off over a length of 30 mm. in order to allow the air to expand again after passing over the horizontal surfaces of the models. In this way, intense noise due to air vibrations downstream was removed.

The wedges were fitted with a number of static pressure tubes. To each wedge a dynamic pressure tube was fitted for supersonic tests only : in the supersonic tests, the flow downstream of the shoulders of the wedges was always supersonic, so that the tube and its mounting could not affect the conditions upstream. The positions of the tubes on the wedges are shown in the sketch in Fig. 25.

For the subsonic experiments, each wedge was mounted in the tunnel by means of three screws, passing through the tunnel walls into the side of the wedge, and placed well back from the apex so that no obstruction occurred which could affect conditions upstream. A careful fitting of rubber was made between the wedge and the faces of the tunnel side windows (the rubber being cut to the shape of the wedge), so that there should be a minimum of disturbance at the steel and glass junction. The tunnel side windows were of special optical glass, with an intrinsic zero error of not more than two-thirds of a fringe.

For supersonic tests it was found necessary to support the models more firmly, and the method adopted is shown in Fig. 24, which also shows the mounting in the tunnel of the nozzle with a theoretical Mach number of 2·8.

6. *Subsonic Tests.*—6.1. For the series of tests at subsonic speeds the tunnel was partially evacuated. This was to reduce the number of fringes and so to facilitate evaluation. The pressure in the settling chamber was approximately 0·4 atmospheres. It was not possible to dry the air, but no use has been made in this report of tests for which it was necessary to heat the air in order to remove condensation.

During the running of the tunnel simultaneous photographs were taken of the interference patterns and the manometer board. The Mach number of the incident flow was calculated from manometer measurements of the static pressure at the beginning of the working section, well upstream of the model.

6.2. *Discussion of Results.*—A selection of the photographs is given in Figs. 3 and 4, and the results of the evaluations of these are shown in Figs. 5 and 6.

In the neighbourhood of $M = 0{\cdot}7$ for the incident flow sound speed is reached at the shoulder of the wedge, and a small region of supersonic flow exists downstream of it. This region increases with increase of Mach number, and at the highest speeds a shock wave is to be seen at some distance down the horizontal surface, the distance increasing with M_1. A shock wave is represented by a large superposition of density contours, as is to be expected ; it is not to be confused with a discontinuity of density gradient such as is to be seen in photograph 5768 (Fig. 4) just at the end of the expansion round the shoulder, although such a discontinuity may eventually lead to a shock wave, as is the case here, at some distance out in the field.

A waviness in the density contours can be seen just behind the shoulder in photograph 6009 (Fig. 3) for the 20 deg. wedge, and in photographs 5722, 5750 (Fig. 4) for the 40 deg. wedge ; it is not present for the highest Mach numbers (6023, 5768). This phenomenon is probably caused by a shock wave produced by an air bubble at the corner, where the boundary layer cannot turn sufficiently quickly. This difficulty is overcome when the velocity of the incident flow is great enough, and as we have the velocity of sound reached at (or very near to) the shoulder, a radial (Meyer) expansion in supersonic flow takes the flow round the corner. This is quite clear in photograph 5768, where the shock wave caused by the blockage in the tunnel (as in 6023 for the 20 deg. wedge) has moved a long way down the surface of the wedge. The sequence of sharp corners in the contour lines represents a discontinuity in the density gradient at the end of the expansion : but it does not imply a discontinuity of density. Far out from the model however, the contours are closing in to form a discontinuity of density (i.e., a shock wave), which will run into the main blockage shock wave. Downstream of the Meyer expansion one would predict theoretically a nearly uniform flow at supersonic speed : a compression of the flow is in fact observed, and this is due to the blockage effect. The ability of a shock wave to increase the boundary layer thickness and cause breakaway of the flow may be seen clearly by the interferometer technique.

The lines of constant density along the sloping edge, where the boundary layer is not enough to affect the photographs, appear to spring normally from the surface of the wedge ; furthermore, as we have already remarked, the sonic line appears to occur very close indeed to the shoulder. Both these findings support the theoretical work of Maccoll and Codd[3] who predicted that such was the case. Their assumption that the sonic line itself begins normally to the sloping edge is well supported, although it is difficult to trace lines in the neighbourhood of the corner itself, and there is also some optical distortion at such a point of steep density gradient.

Maccoll and Codd have concluded, on the above theoretical considerations, that, once the sonic condition has been established at the corner of a wedge, the maximum Mach number obtained in the flow round the corner is independent of the Mach number of the incident flow. The values calculated for these limits were $M = 1{\cdot}46$ for the 20 deg. wedge, and $M = 1{\cdot}78$ for the 40 deg. wedge. The values of the maxima can be deduced very accurately by the interference method, given the Mach number of the incident flow, since the number of fringes at the corner can be counted well out in the field, where the difficulties of crowding and optical distortion do not exist. In this way the curves of Fig. 9 have been obtained from a number of tests. The two sets of points given for each of the tests 57 and 60 are derived from the use of different manometer readings as the basis of the evaluations (one on the back of the wedge and one on the sloping edge). It will be seen that the theoretical maximum Mach number is not achieved up to $M = 0{\cdot}8$—that the maximum obtained increases with M_1. This may be due, at least in part, to the decrease in the effective angle of expansion at the corner caused by the inability of the boundary layer to turn quickly enough, an effect which, as stated above, would be expected to diminish with increasing M_1.

The values of p/p_1, calculated from the photographs, are given in Figs. 5 and 6. In Figs. 7 and 8 are shown the lines of constant velocity, drawn at equal intervals $0{\cdot}1$ of the Mach number, for two tests on the 20 deg. wedge and the 40 deg. wedge respectively.

7. *Supersonic Tests.*—7.1. A series of nozzles was available for tests at supersonic velocities. These nozzles had been calculated for shape by the method of characteristics, and were designed to produce uniform parallel flow without shock waves. If one assumes sonic velocity perpendicular to the throat section, the one-dimensional theory of flow in nozzles then gives accurately the exit velocity. If A_c is the area of the throat in the tunnel, and A_e the exit area of the parallel stream,

$$\frac{A_e}{A_c} = \frac{1}{M_1}\left\{\frac{(\gamma - 1)\,M^2 + 2}{\gamma + 1}\right\}^{(\gamma+1)/2(\gamma-1)} \qquad (11)$$

The theoretical Mach numbers of the nozzles used were $1{\cdot}4$, $2{\cdot}0$ and $2{\cdot}8$.

The tunnel was run without evacuation or compression for the $M_1 = 2{\cdot}0$ and $M_1 = 2{\cdot}8$ nozzles, but it was necessary partially to evacuate the tunnel in order to obtain supersonic flow with the $M_1 = 1{\cdot}4$ nozzle.

The tunnel has a flexible second throat, but, as the latter caused difficulties on account of vibrations, and it was found possible to carry through the experiments without it, it was not used.

A check on the Mach number could be obtained by means of the manometer record of pressures in the working section and settling chamber, when pressure holes were suitably placed for the former ; further checks could be made by measuring the angle of the shock wave when this was attached to the tip of the wedge, and by measurement of the angle of the wavelets from small disturbances set into the nozzle when the tunnel working section was empty. These methods, however, are not sufficiently accurate in themselves, and the calculations given in Figs. 12, 13, 16, 17, 20 and 21 are based on the assumption of the theoretical Mach number, and the theoretical loss of total head, and then are found by assuming as correct a manometer reading on the horizontal wedge surface and working back from it to the shock wave. The calculated distribution is then compared with the theoretical distribution, given as a dotted line for those cases where the wave is attached to the tip. It was found that the best agreement occurred with the assumption of the theoretical Mach number (to the nearest $0{\cdot}1$). The pressure coefficient used is the usual one, p/p_1.

7.2. *Discussion of Results.*—(Figs. 15, 18, 19.) The photographs taken with the two nozzles of higher Mach number show clearly the theoretically known features of such purely supersonic flows. The shock wave is attached to the tip of the wedge, and the flow along the horizontal surface is uniform, shown by the absence of fringes. At the shoulder there is a Meyer expansion, for which density is constant along a radius vector from the corner. The shock wave extends from the tip in a straight line until it meets the expansion, when it begins to curve.

It was found that the photographs obtained with the $M_1 = 2{\cdot}0$ nozzle were exactly reproducible on different days, but with the $M_1 = 2{\cdot}8$ nozzle the flow did not remain entirely steady even during an individual run (*see* Figs. 18 and 19) ; evaluation of different photographs for the latter did not however reveal any great variations. The agreement between the theoretical and experimental distributions is seen to be good, using the method of approach described in 7.1 above, despite the fact that the air had not been dried.

A number of tests were carried out for each nozzle with an empty working section, in order to examine the quality of the flow. Some of the photographs are reproduced in Fig. 23 which shows the boundary layer effect quite clearly. In photograph 7102 one can see the disturbance which arises where the nozzle ends and wooden end pieces are fitted to conduct the flow into the diffuser. In general it is seen that the flow is remarkably steady, and free from disturbances of any magnitude, especially condensation shock waves, which are the usual sources of loss of performance with nozzles in supersonic flow. There is some disturbance near the axis for $M_1 = 2{\cdot}8$, and this may be the cause of the unsteadiness near the wedge tip to be observed in Figs. 18 and 19. The thickness of the shock waves observed must be attributed to the slight deviation from parallelism in the light passing through the tunnel.

For the 40 deg. wedge, with $M_1 = 1{\cdot}4$, the shock wave is detached from the tip (Fig. 11), as was to be expected, since this Mach number lies well below the critical value for attachment. The flow behind is subsonic, and this may be compared in form with the flow at subsonic speeds.

The speed of sound is reached at or near the shoulder of the wedge, and a Meyer expansion follows round the corner. At the limit of the expansion there is a discontinuity in pressure gradient which develops into a shock wave at a little distance from the corner. There is a positive pressure gradient along the upper surface of the wedge. The results of the evaluation are given in Fig. 13.

For the 20 deg. wedge, the critical Mach number for detachment of the shock wave is $M = 1{\cdot}41$. With the nozzle of theoretical Mach number $1{\cdot}4$, we obtained photographs of flow with the

wave attached, and, on other occasions, detached. These are shown in Fig. 10. The type of flow follows the lines of that described for the 40 deg. wedge, the flow behind the shock wave being subsonic. The evaluation is given in Fig. 12.

By cutting off the light from that arm of the interferometer which did not pass through the wind tunnel, it was possible to take shadow photographs of the flow. The sharp refraction of the light in a shock wave led to a loss of light in the collecting mirror and hence to a dark line in the photograph. Some of these examples have been included among the figures (*see* Figs. 10, 11, 18 and 19). The discontinuity arising near the shoulder with the subsonic flow behind the shock wave ($M_1 = 1{\cdot}4$) can be seen clearly in photograph 11618 (Fig. 11).

For the $M_1 = 1{\cdot}4$ nozzle it was possible to photograph conditions at or near the throat. In Fig. 22 photographs are given of the density contour lines during the running up of the tunnel. After sonic velocity has been reached at the throat, but before the pressure ratio built up is sufficient to produce supersonic flow in the whole of the nozzle, a shock wave occurs in the nozzle on the downstream side of the throat. We see it beginning as a small shock wave near the nozzle walls, then spreading across the whole section of the nozzle and moving simultaneously downstream as the pressure difference across the ends of the nozzle is increased. In photograph 11230 the supersonic flow has been established. Important to note is the shape of the density contours in the throat in this photograph, giving as it does the qualitative shape of the sonic line.

7.3. *Wedge Resistance.*—In Fig. 14 are compared the pressure coefficients p/p_1 for the 40 deg. wedge at the supersonic velocity $M_1 = 1{\cdot}4$ and at three subsonic velocities. Maccoll and Codd, in their report quoted, came to the conclusion that the resistance of a wedge could be computed with sufficient accuracy in the range $M_1 = 0{\cdot}7$ to $1{\cdot}5$ from the assumption that the curve of p/p_1 is the same over this range of velocities. The basis of their argument was that p/p_1 had a fixed value at the stagnation point at the tip of the wedge, and another fixed value at the shoulder on the assumption of sonic velocity there. Fig. 14 supplies adequate justification for this conclusion, remembering that the fluid resistance arises only from the sloping edge.

It is also of interest to observe the striking similarity between the pressure curves over the whole wedge for $M_1 = 1{\cdot}40$ and $M_1 = 0{\cdot}803$. Since the Mach number of the flow on the axis immediately behind the shock wave is approximately $0{\cdot}7$, a somewhat higher Mach number was to be expected for the corresponding subsonic pressure field, since at the same point in the field of the latter flow the presence of the stagnation point would already have caused an appreciable reduction of the axial velocity.

Acknowledgements.—The author is indebted to the Chief Scientist, Ministry of Supply, for permission to publish this paper.

Mr. F. W. Jackson assisted the author in the direction of the wind tunnel, and, as has already been stated in the introduction, the interferometer was set up and operated by Dipl.-Ing. W. Richter, assisted by Herr G. Klages and Herr Enge ; the calculations from the interference photographs were carried out by Dr. E. Groth, Herr H. Thiel and Frl. I. Müller.

REFERENCES

No.	*Author*	*Title, etc.*
1	Groth	The Measurement of the Flow around an Aerofoil by means of a Mach-Zehnder Interferometer. M.A.P. Völkenrode Report R. & T. 127 (Jan. 1946).
2	Groth	On the Evaluation of the Density Field at High Subsonic Speeds measured with an Interferometer. UM 2059 (in German); M.A.P. Völkenrode Translation No. R. & T. 96 (with 2 appendices added).
3	Maccoll and Codd ..	Theoretical Investigations of the Flow around Various Bodies in the Sonic Region of Velocities. M. of S. A.R.D. Theoretical Research Report No. 17/45. A.R.C. 9315. September, 1945. (Unpublished.)
4	Durand (editor) ..	Aerodynamic Theory. Vol. III. 1935. Julius Springer. Berlin.
5	F. Schubert	Zur Theorie des stationären Verdichtungsstosses. ZAMM Vol. 23 (1943), Part 3, pp. 129–138.
6	Zöbel	Stromungsmessung durch Lichtinterferenz. FB 1167 (in German); M.A.P. Völkenrode Translation R. & T. 384.

APPENDIX

Sensitivity and Accuracy of the Interference Method applied to Pressure Measurements in Wind Tunnels

By

E. Groth

1. *Introduction.*—The interferometer of Mach Zehnder has been successfully used for measuring the pressure distribution for two-dimensional flow around an aerofoil mounted in a wind tunnel. The rays of the light used are parallel to the span of the model and get a phase shift which is proportional to the local density in the tunnel. If the breadth of the working section is denoted by L—this value is also equal to the span of the model—and if the undisturbed Mach number before the model is M_1 and the corresponding density ρ_1, then the fringe shift y/b is related to the local density ρ in the working section by the equation

$$\rho - \rho_1 = \frac{\lambda_v}{L \cdot \frac{n-1}{\rho}} \cdot \frac{y}{b} \quad .. \quad .. \quad .. \quad .. \quad .. \quad .. \quad .. \quad \text{(A.1)}$$

If the mirrors of the interferometer are in such a position that, without a flow in the wind tunnel, the interference fringes are parallel lines of the constant distance b, the fringe shift y can be measured directly from the photographs. If $b = \infty$, the fringes arising from the flow around the model represent curves of constant density, and between two consecutive fringes $\Delta y/b = 1$. Because of the simpler evaluation and greater ease of interpretation, photographs with these curves of constant density are generally used.

λ_v is the wavelength of the light used, $\frac{n-1}{\rho} = 0{\cdot}00222$ is constant for air.

If we introduce a dimensionless shift coefficient c_s

$$c_s = \frac{\rho - \rho_1}{\rho_1} = A \cdot \frac{\rho_0}{\rho_1} \cdot \frac{y}{b}, \qquad A = \frac{\lambda_v}{L \dfrac{n-1}{\rho} \rho_0} \quad .. \quad .. \quad .. \quad (A.2)$$

where ρ_0 is the density in the settling chamber, we obtain for the pressure coefficient p/p_1 the equation

$$\frac{p}{p_1} = (1 + c_s)^\gamma \quad .. \quad .. \quad .. \quad .. \quad .. \quad .. \quad .. \quad .. \quad (A.3)$$

This formula must be amended, if a loss of total head occurs, e.g., by a shock wave. We introduce the magnitude

$$\varepsilon = \left\{\frac{p_0}{p_0'}\right\}^{\gamma-1} - 1, \qquad (\gamma = 1{\cdot}405) \quad .. \quad .. \quad .. \quad (A.4)$$

and write $\varkappa = p_0'/p_0$ for the measure of the loss of total head. At supersonic flow (F. Schubert[5]) $\varkappa$ is a function of $M_1 \cos \alpha$, where α is the angle between the normal to the shock wave and the direction of flow ahead of it. In Fig. 26 ε is plotted as function of $M_1 \cos \alpha$. Instead of equation (A.3) we get for the pressure coefficient

$$\left\{\frac{p}{p_1}\right\}' = (1 + \varepsilon)\,(1 + c_s)^\gamma \quad .. \quad .. \quad .. \quad .. \quad .. \quad .. \quad (A.3')$$

In these formulae the values behind the shock wave are denoted by a dash.

2. *Sensitivity and Accuracy of the Method.*—2.1. If we consider the whole Mach range $0 < M_1 < \infty$ we have at very low subsonic speeds, and also at very high supersonic speeds, only small density changes in the wind tunnel. In the one case the flow is nearly incompressible, in the other the absolute value of the density becomes so small, that only small changes are possible. As the interferometer measures density changes, the question must be discussed, up to what limits the method is still applicable. Therefore the fringe shifts will be calculated for the maximum possible density changes in a wind tunnel.

2.2. In the direction of increasing pressure the limit is given by the stagnation point, for which, at supersonic velocities, the loss of total head caused by a vertical shock must be taken into account. From equation (A.2) we get

$$\left(\frac{y}{b}\right)_{\text{st. p.}} = \frac{1}{A}\left(\varkappa - \frac{\rho_1}{\rho_0}\right).$$

This fringe shift and the corresponding pressure coefficient $(p/p_1)_{\text{st. p.}}$ are plotted in Fig. 27. From the tests in the wind tunnel A 7 we take for the constant A the value 0·0132.

2.3. A natural limit in the direction of lower pressure does not exist, but it will be sufficient to calculate the fringe shift for a local velocity which corresponds to the double value of the Mach number of the undisturbed flow. This gives for incompressible flow a pressure coefficient $\Delta p/q = -3$ ($q = \frac{1}{2}\rho v^2$ = dynamic pressure); for $M_1 = 0{\cdot}8$ it is well known that there has never been observed a local Mach number higher than $M = 1{\cdot}6$; and at supersonic speeds an expansion of the flow through from 30 to 40 deg. leads to the double Mach number.

We obtain the formula

$$\left(\frac{y}{b}\right)_{2M_1} = \frac{1}{A \dfrac{\rho_0}{\rho_1}} \left\{ \left(\frac{1 + \dfrac{\gamma - 1}{2} M_1^2}{1 + 2(\gamma - 1) M_1^2} \right)^{1/(\gamma - 1)} - 1 \right\}$$

This fringe shift and the corresponding pressure coefficient are plotted in Fig. 28.

From these two diagrams we see that, if we demand a shift of at least ten fringes as necessary to obtain sufficient points for an evaluation, we must (with our factor $A = 0{\cdot}0132$) restrict ourselves to the Mach range $0{\cdot}54 \leqslant M_1 \leqslant 3{\cdot}8$ with respect to the stagnation point and to $0{\cdot}32 \leqslant M_1 \leqslant 2{\cdot}4$ with respect to the maximum velocity in excess of M_1. From these two limits we can take the mean value $0{\cdot}4 \leqslant M_1 \leqslant 3{\cdot}2$.

2.4. The maximum sensitivity of the interference method lies between $M_1 = 1{\cdot}0$ (for the excess velocities) and $1{\cdot}6$ (for the stagnation point). As wind tunnel tests are not possible in the immediate neighbourhood of $M_1 = 1$, we get the result that an interferometer has its maximum sensitivity in a wind tunnel at the maximum possible subsonic and the minimum possible supersonic velocity. The same fringe shift to the stagnation point (*a*) and to the point of double velocity (*b*) at subsonic and supersonic flow can be seen from the following table.

TABLE 1

Subsonic M_1	Supersonic M_1	
	(*a*)	(*b*)
0·4	4·50	2·10
0·5	4·00	1·80
0·6	3·57	1·55
0·7	3·24	1·36
0·8	2·96	1·19
0·9	2·73	1·08

The small sensitivity of the interference method in the direction of increased velocities for a supersonic flow is to be noted.

2.5. The accuracy of the method must be discussed from the point of view of what changes in density and pressure belong to a shift of one fringe. In this case we get the formulae

$$\left(\frac{\rho}{\rho_1}\right)_{y\,b\,=\,1} = 1 + A \cdot \frac{\rho_0}{\rho_1}; \quad \left(\frac{p}{p_1}\right)_{y/b\,=\,1} = \left(1 + A \cdot \frac{\rho_0}{\rho_1}\right)^{\gamma}; \quad \left(\frac{\Delta p}{q}\right)_{y/b\,=\,1} = \frac{2}{\gamma M_1^2}\left\{\left(1 + A \cdot \frac{\rho_0}{\rho_1}\right)^{\gamma} - 1\right\}$$

The percentage errors $100\,\frac{\rho - \rho_1}{\rho_1}$, $100\,\frac{p - p_1}{p_1}$ and the pressure coefficient $\frac{\Delta p}{q}$ for a shift of one fringe are plotted in Fig. 29 for $A = 0{\cdot}0132$. For subsonic flow the percentage error in the density is always less than 2 per cent., but it increases steeply for supersonic flow. At $M_1 = 3{\cdot}0$ a shift of one fringe represents a change of density of 17 per cent. of the density of undisturbed flow, and at $M_1 = 4{\cdot}0$ it represents 48 per cent. The values for the pressure are higher by the factor γ to the first approximation. The pressure coefficient tends to infinity for $M_1 \to 0$ and $M_1 \to \infty$ and has its minimum $0{\cdot}028$ at $M_1 = 2{\cdot}8$.

Only by very careful wind tunnel tests is it possible to reduce the probable error to less than one fringe. Therefore interference measurements with a value of about $0{\cdot}0132$ for the constant A should only be made in a Mach range of about $0{\cdot}5 \leqslant M_1 \leqslant 3{\cdot}0$ in order to avoid too large inaccuracies. This range has already been found above to be necessary for a shift of at least ten fringes for the maximum and minimum possible pressure change. At these Mach numbers therefore the demands for a sufficient sensitivity and accuracy are satisfied simultaneously.

The Mach range suitable for interference tests can be extended by diminishing the factor A. This is possible by increasing the breadth of the working section of the wind tunnel, by increasing the pressure in the wind tunnel or by reducing the wavelength of the light used.

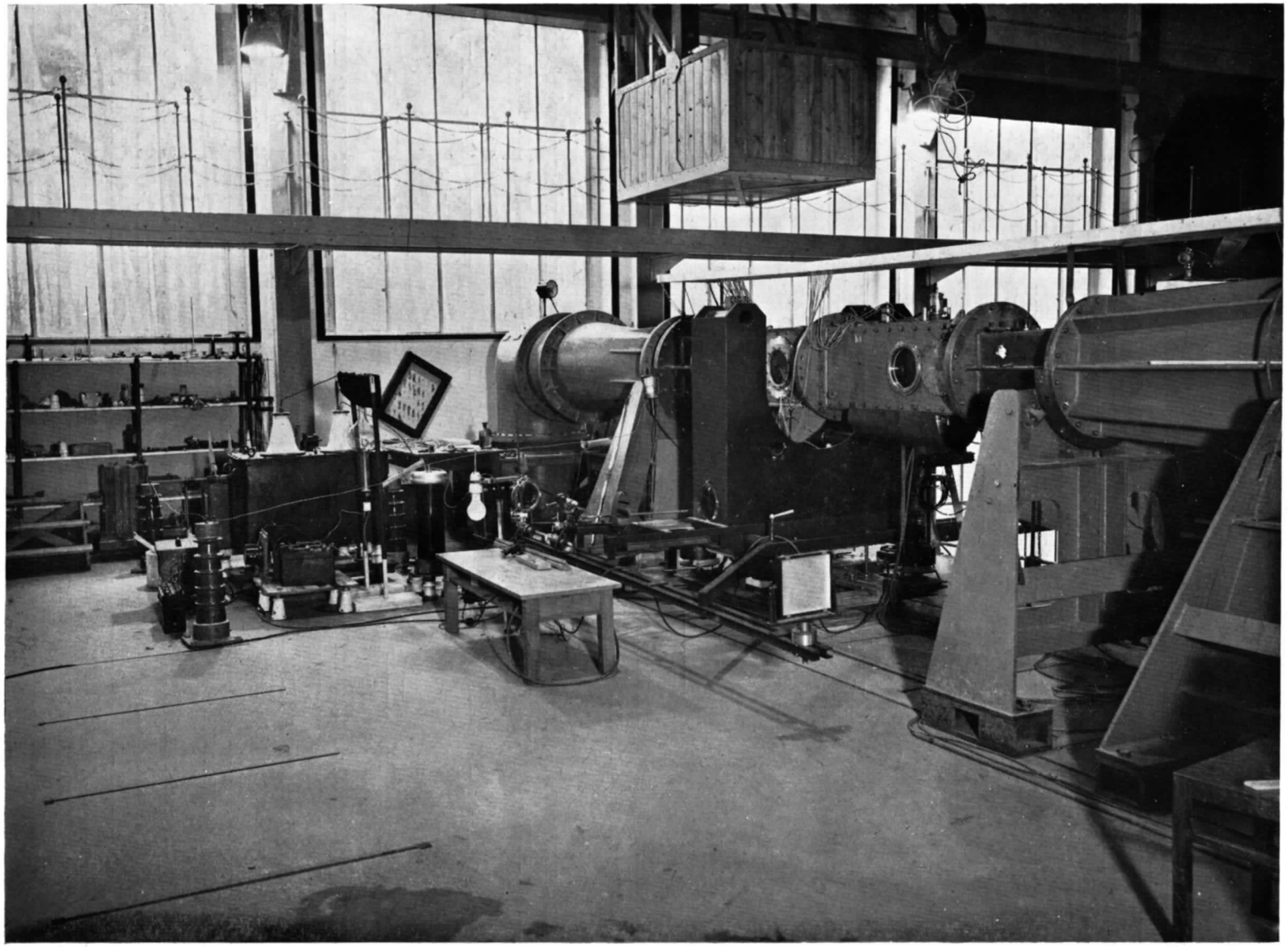

FIG. 2. The Interferometer, the Optical Bench and the Spark Apparatus.

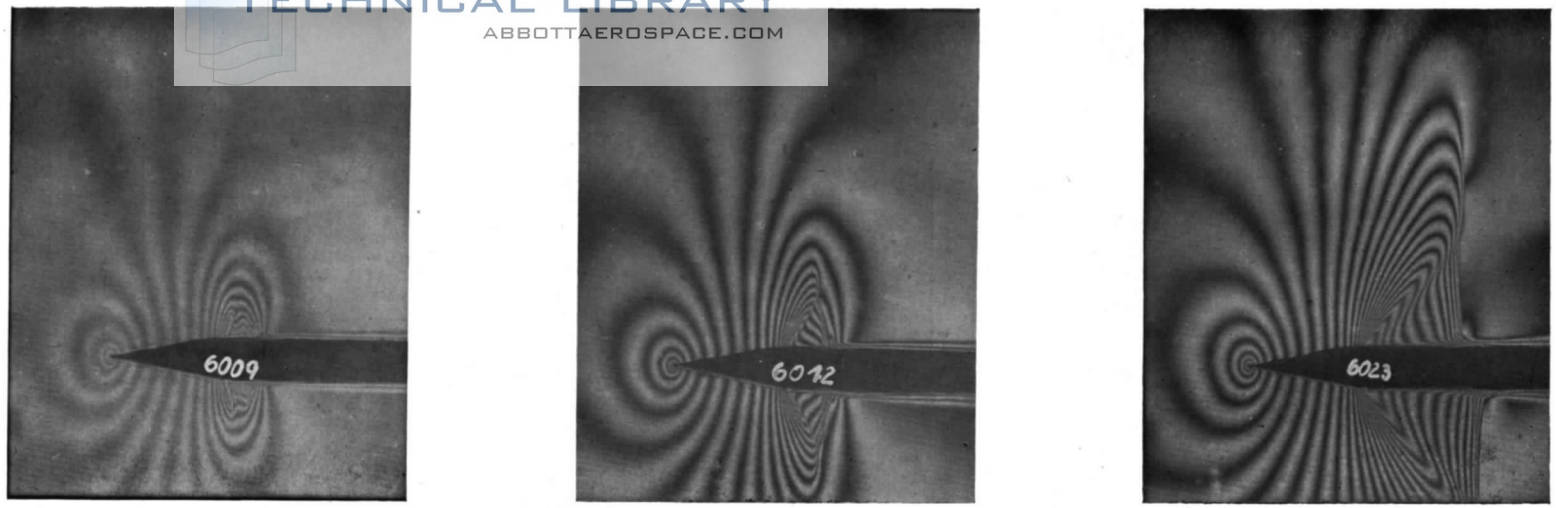

M_1=0.728 M_1=0.768 M_1=0.799

FIG. 3. Density Contour Interference Fringes for a 20° Wedge in a Subsonic Stream.

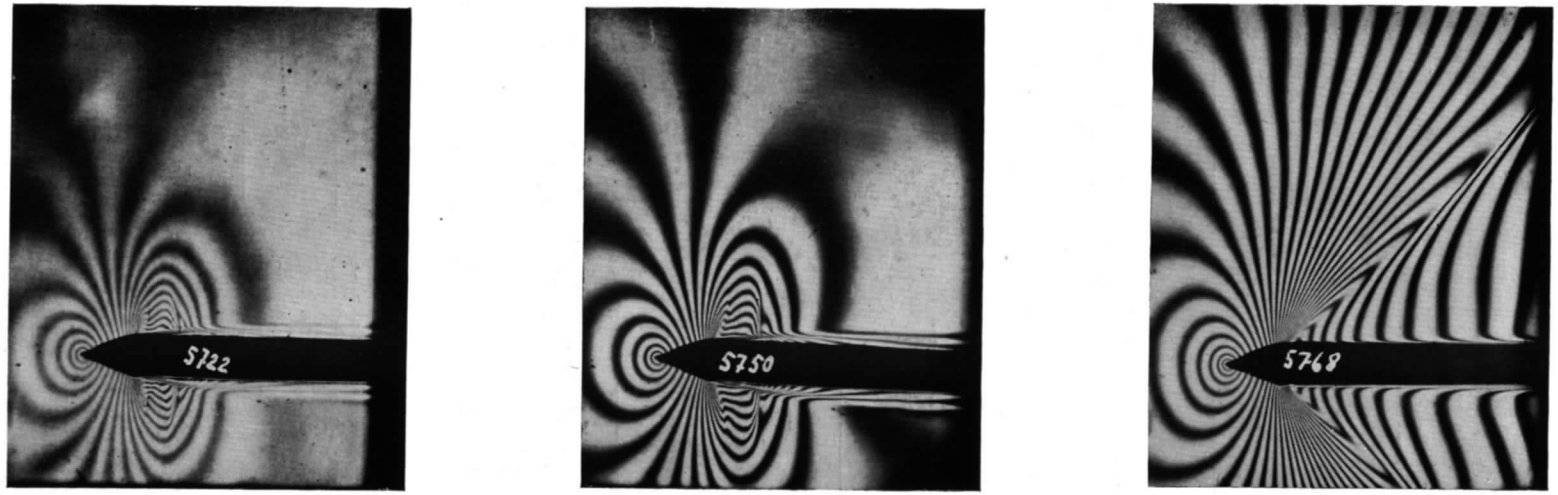

M_1=0.710 M_1=0.734 M_1=0.803

FIG. 4. Density Contour Interference Fringes for a 40° Wedge in a Subsonic Stream.

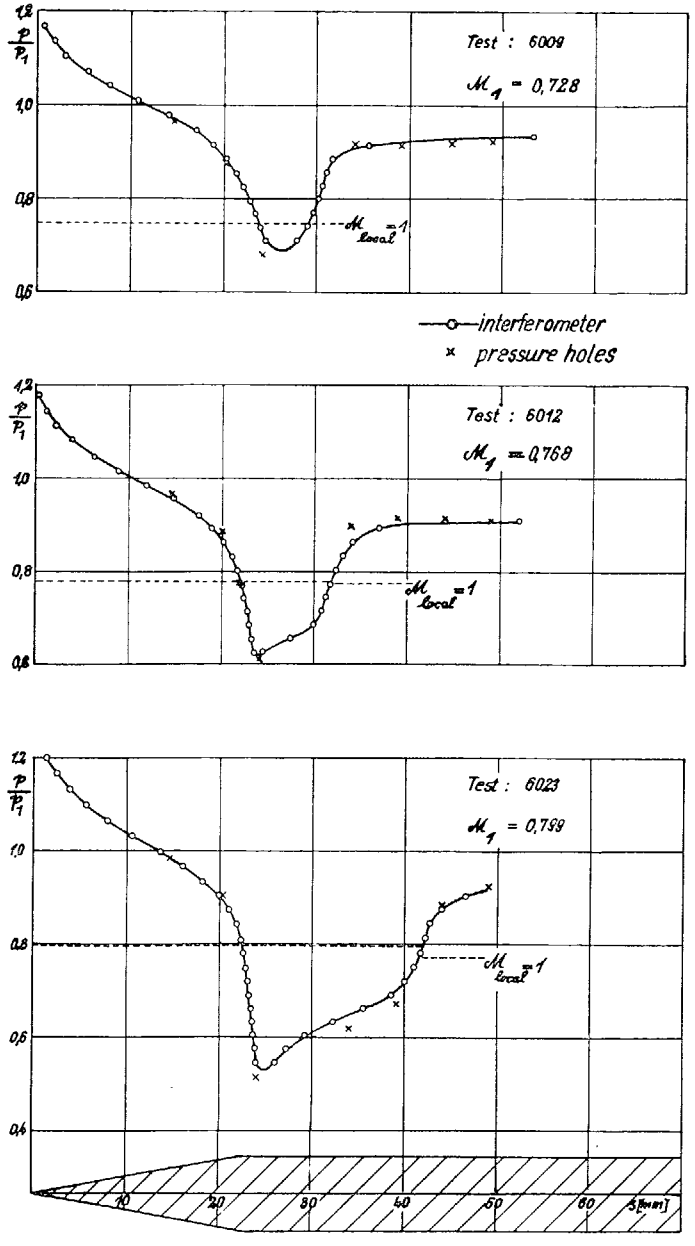

FIG. 5. Pressure Distribution about the 20° Wedge at Subsonic Speed.

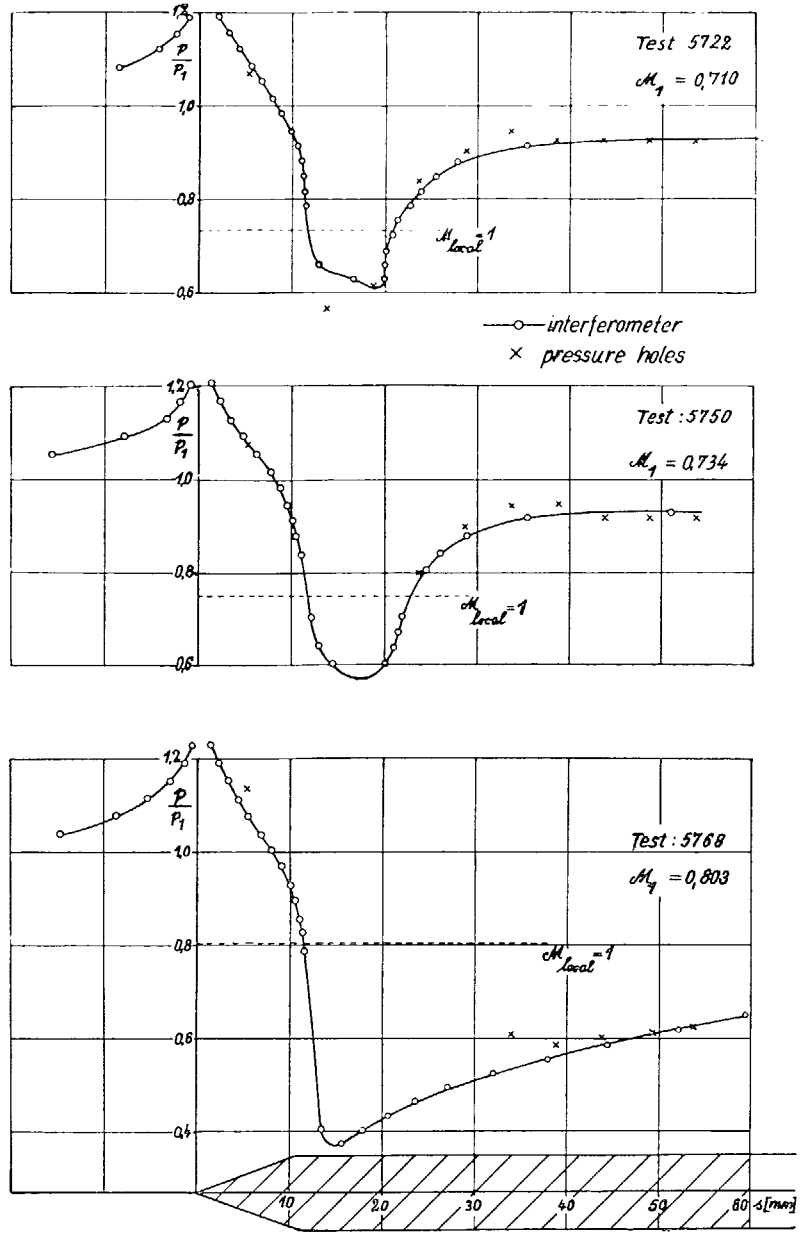

FIG. 6. Pressure Distribution about the 40° Wedge at Subsonic Speed.

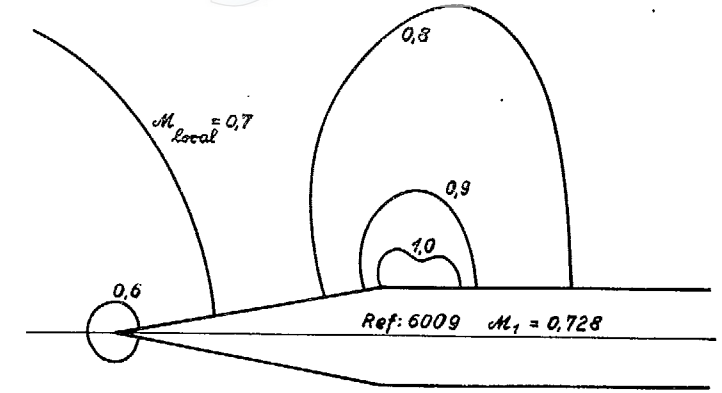

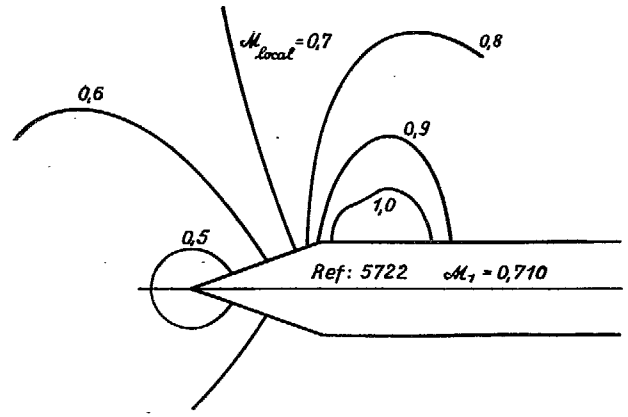

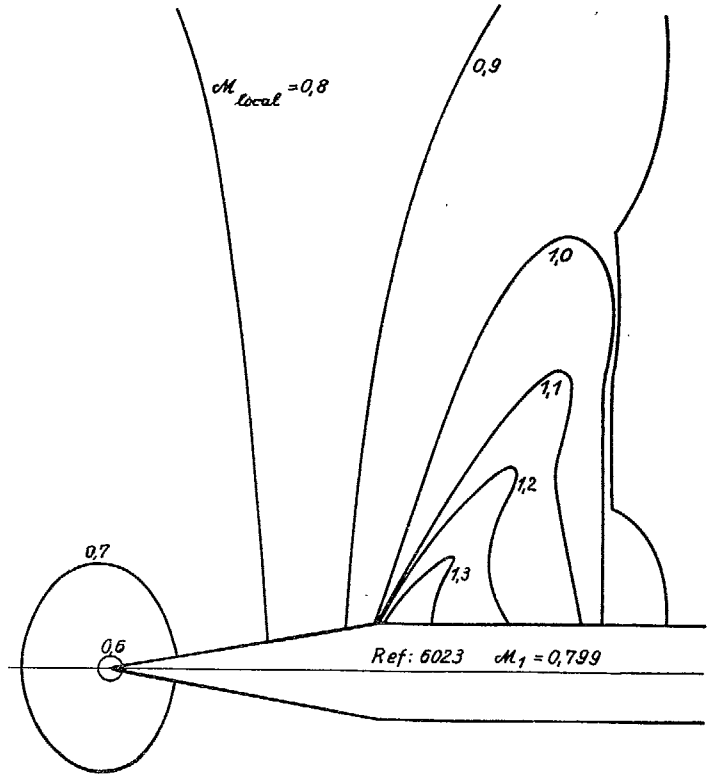

FIG. 7. Mach Number Distribution for 20° Wedge.

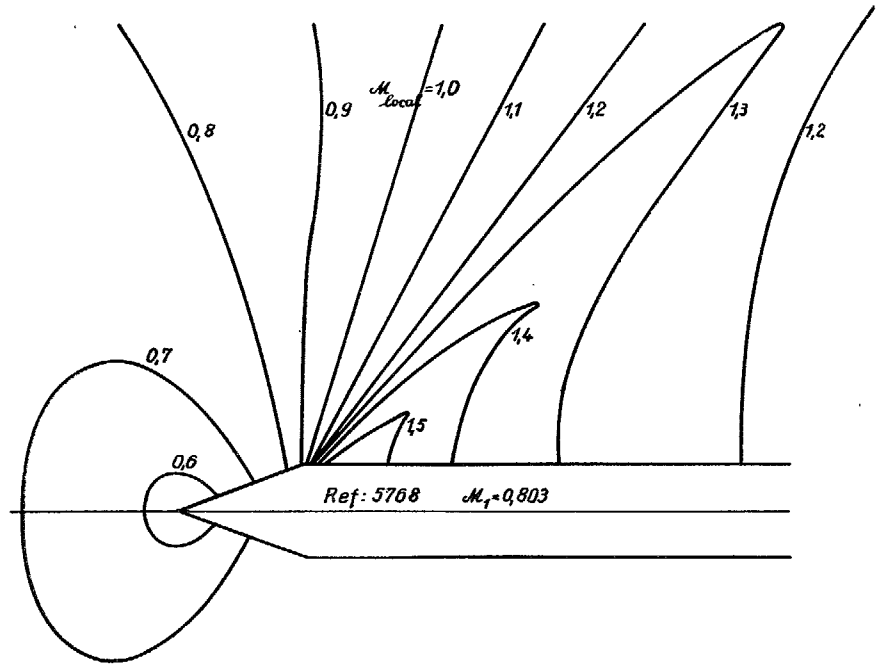

FIG. 8. Mach Number Distribution for 40° Wedge.

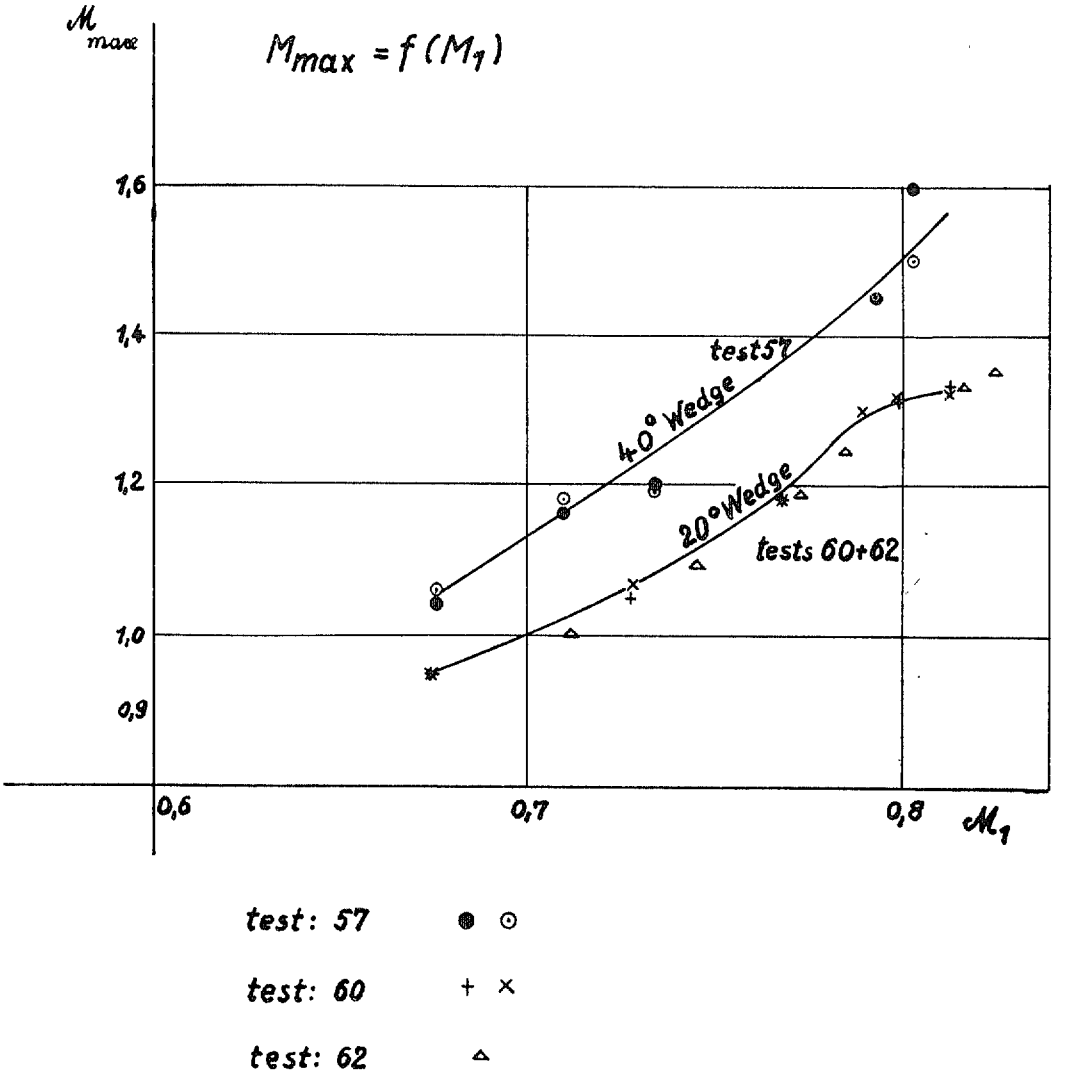

FIG. 9. Maximum Mach Numbers Achieved around Shoulders of Wedges for Varying M_1.

Density contour fringes.

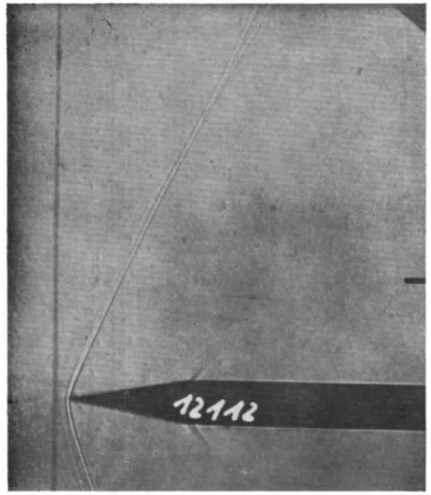

Shadow photograph of attached shock wave.

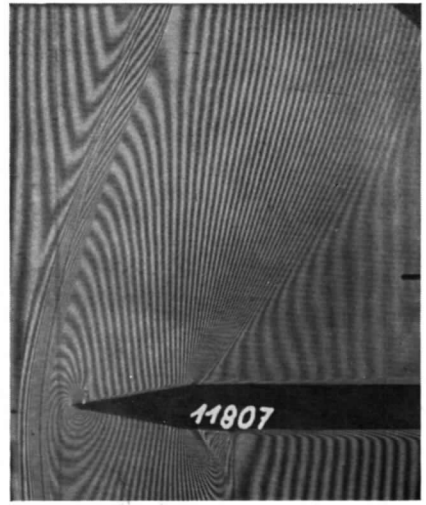

Displacement interference fringes, case of detached shock wave.

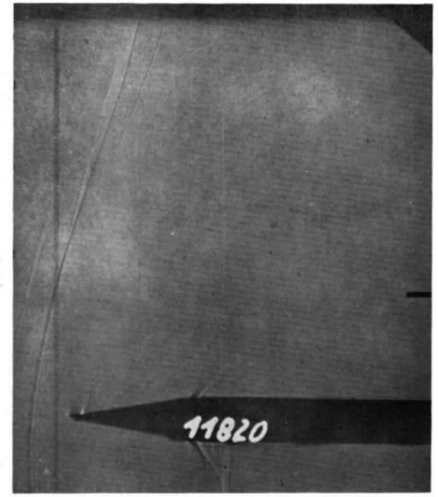

Shadow photograph of detached shock wave.

FIG. 10. Interference Photographs of a 20° Wedge in a Stream of Mach Number 1·4.

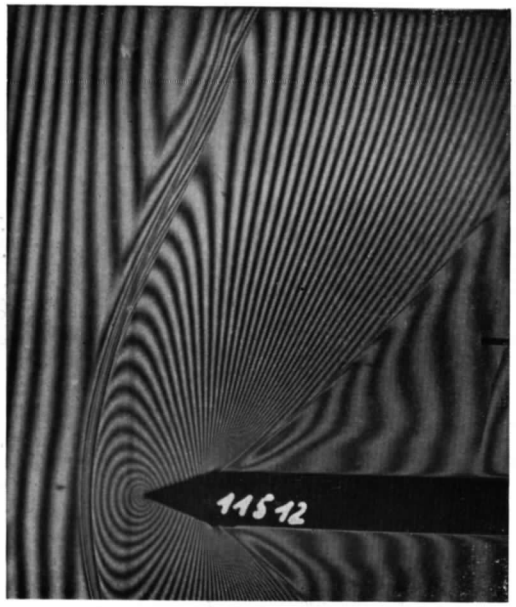

Displacement interference fringes.

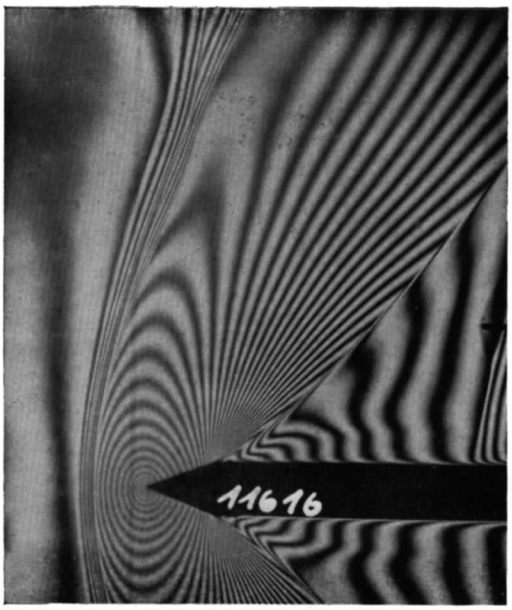

Contour interference fringes.

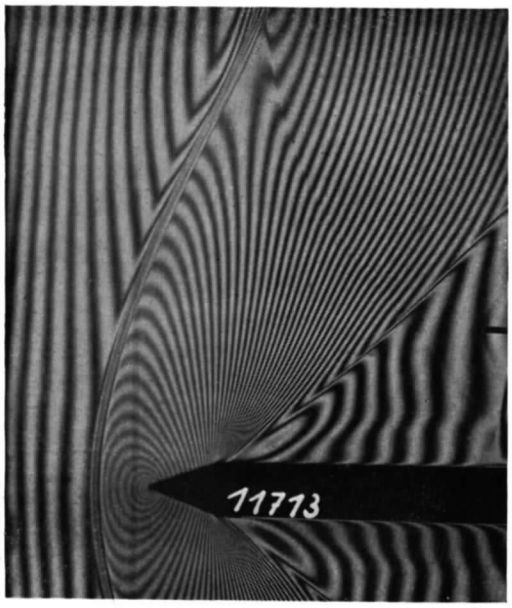

Displacement interference fringes, with the zero interference in a different position.

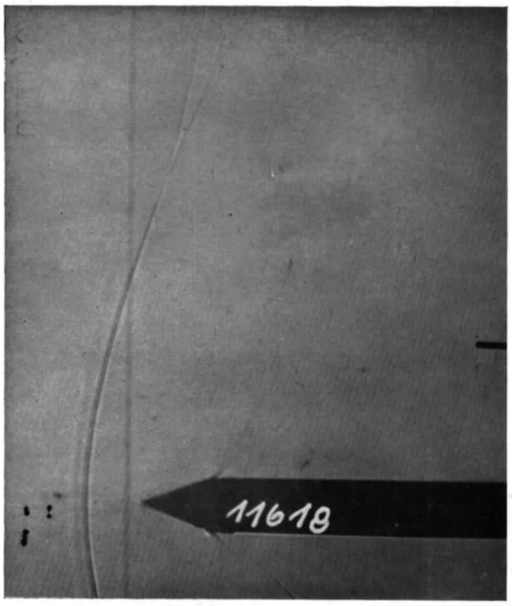

Shadow Photograph.

FIG. 11. Interference Photographs of a 40° Wedge in a Stream of Mach Number 1·4.

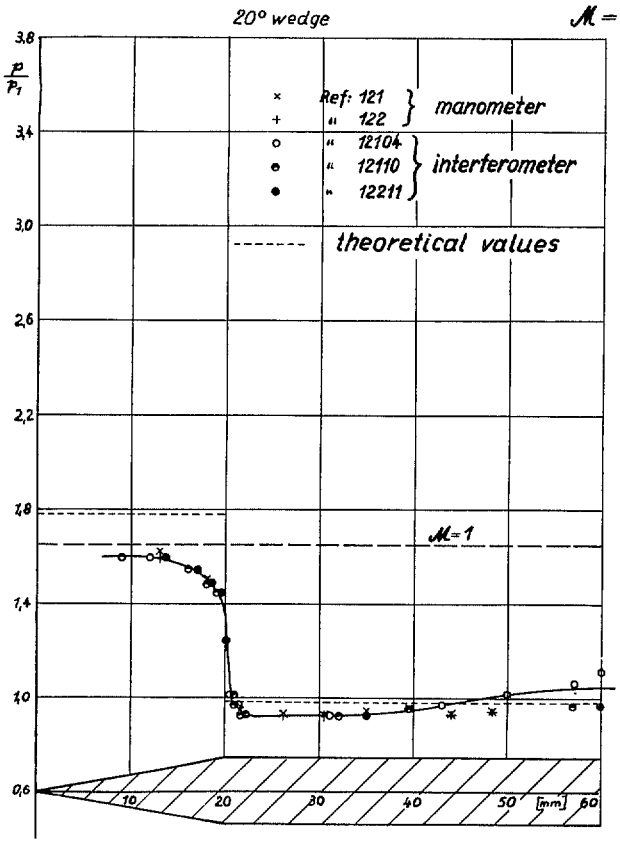

FIG. 12.

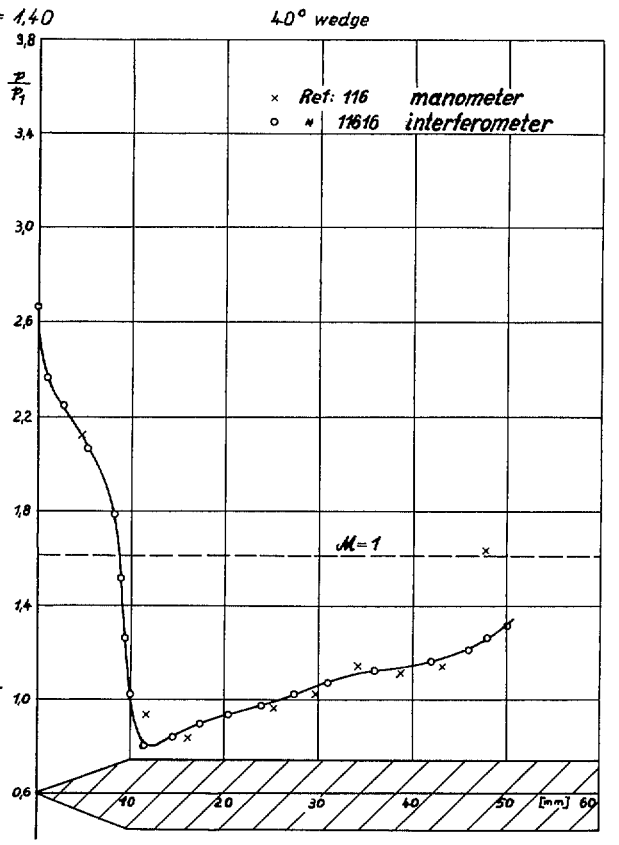

FIG. 13.

Pressure Distribution about the 20° and 40° Wedge at $M_1 = 1{\cdot}40$

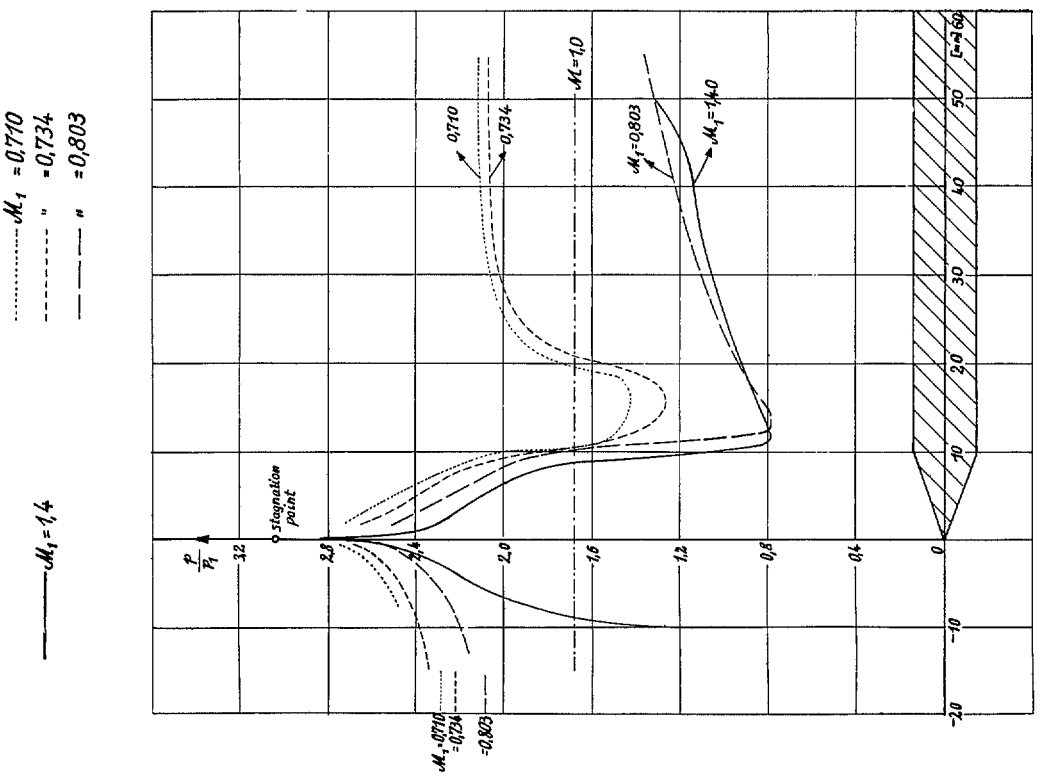

FIG. 14.

Comparison of the Distribution of $\frac{p}{p_1}$ over the 40° Wedge for $M_1 = 1{\cdot}4$ and for Subsonic Speeds.

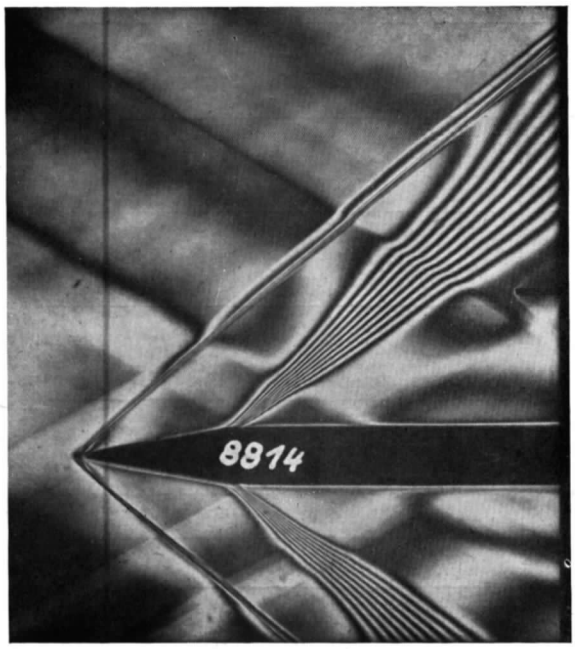

20° wedge contour fringes.

40° wedge contour fringes.

FIG. 15. Interference Photographs for a Stream of Mach Number 2·0.

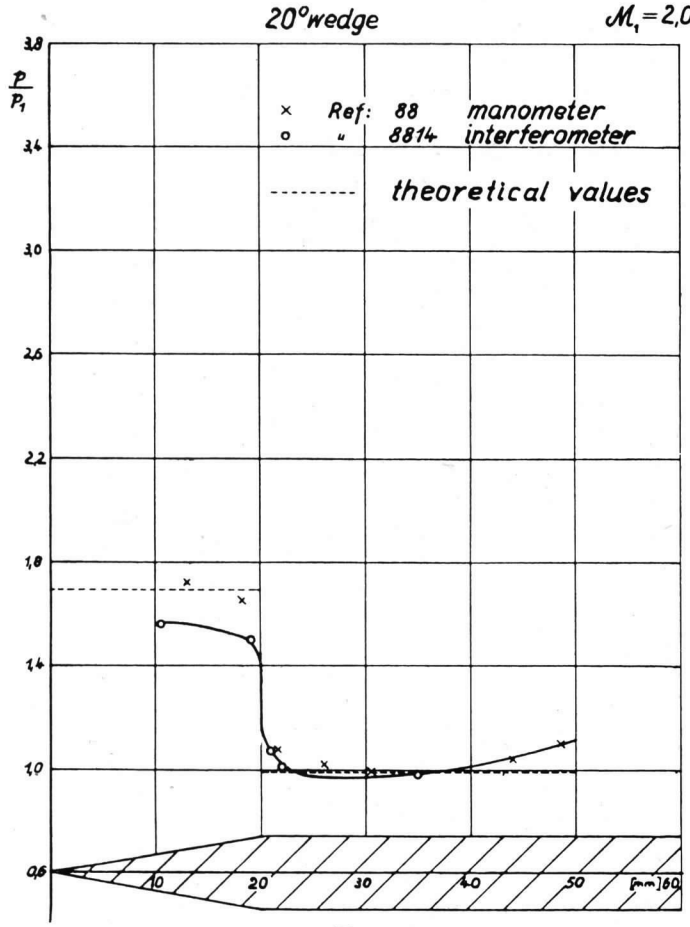

FIG. 16.

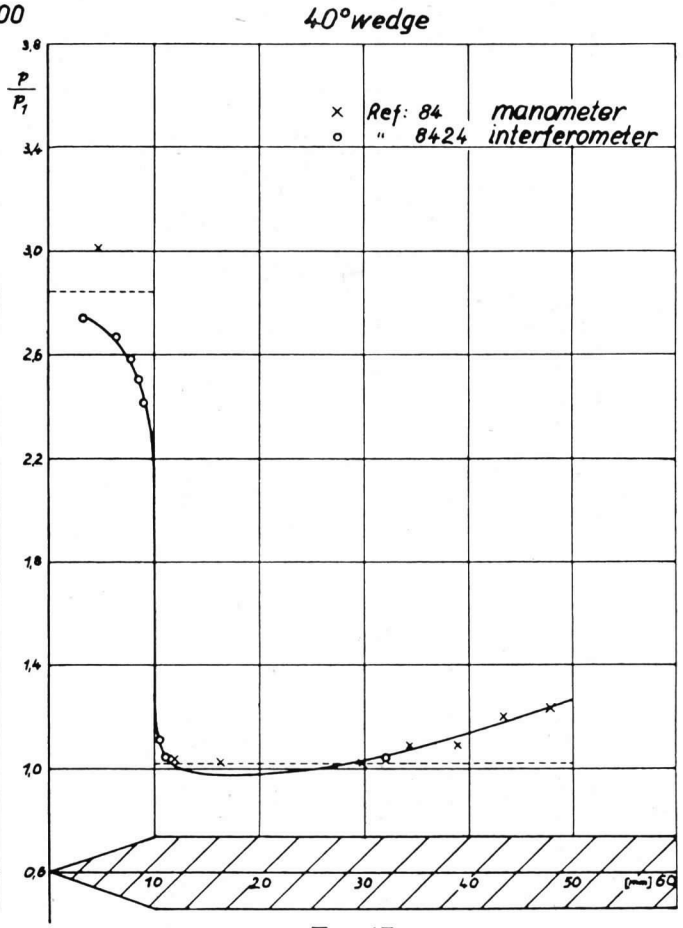

FIG. 17.

Pressure Distribution about the 20° and 40° Wedge at $M_1 = 2{\cdot}00$.

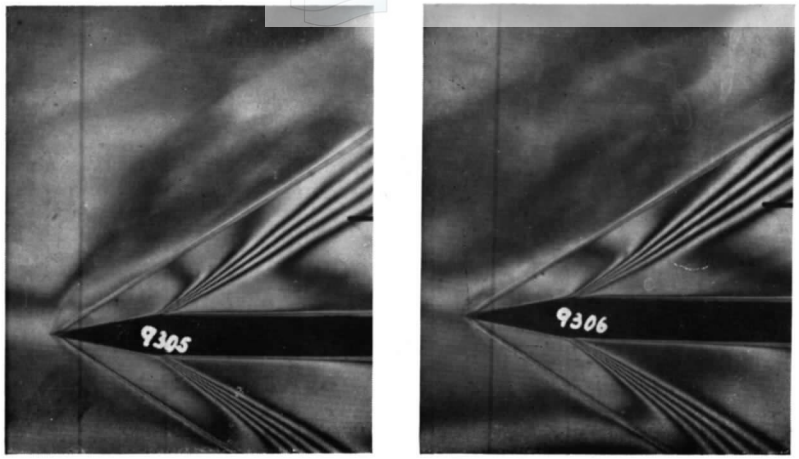

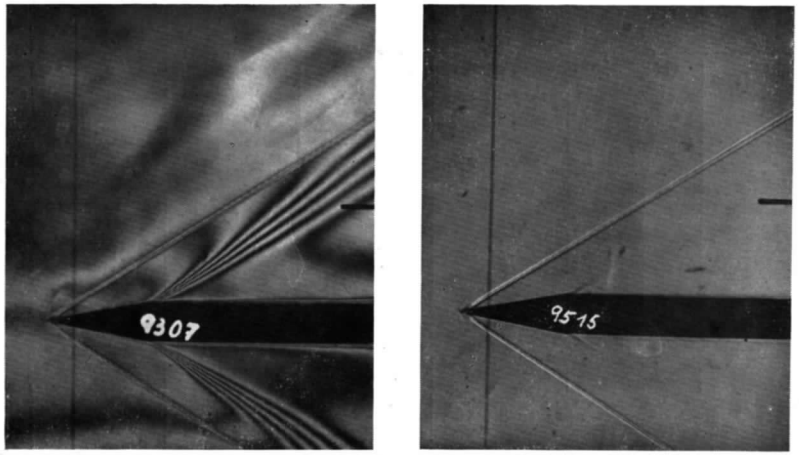

Shadow photograph.

FIG. 18. Interference Photographs of a 20° Wedge in a Stream of Mach Number 2·8.

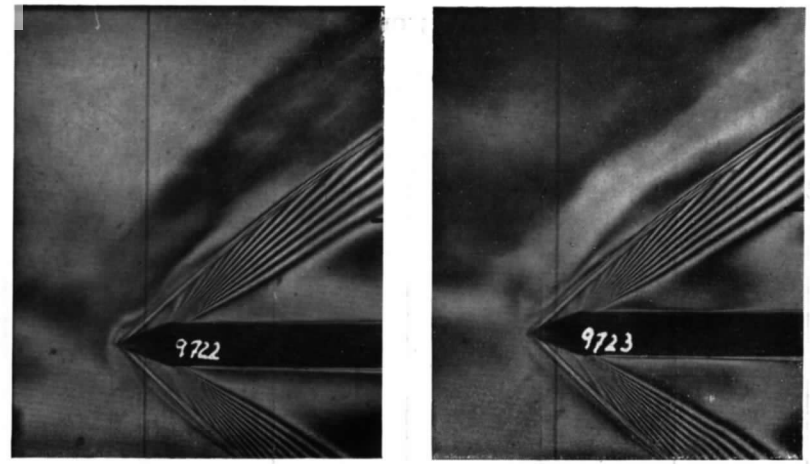

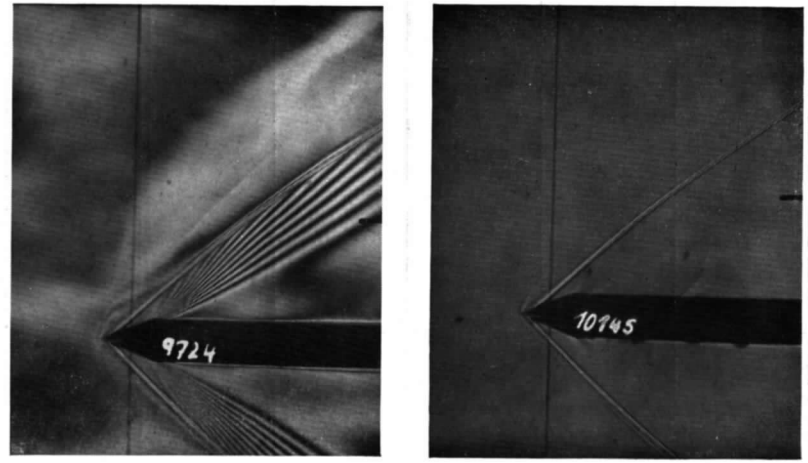

Shadow photograph.

FIG. 19. Interference Photographs of a 40° Wedge in a Stream of Mach Number 2·8.

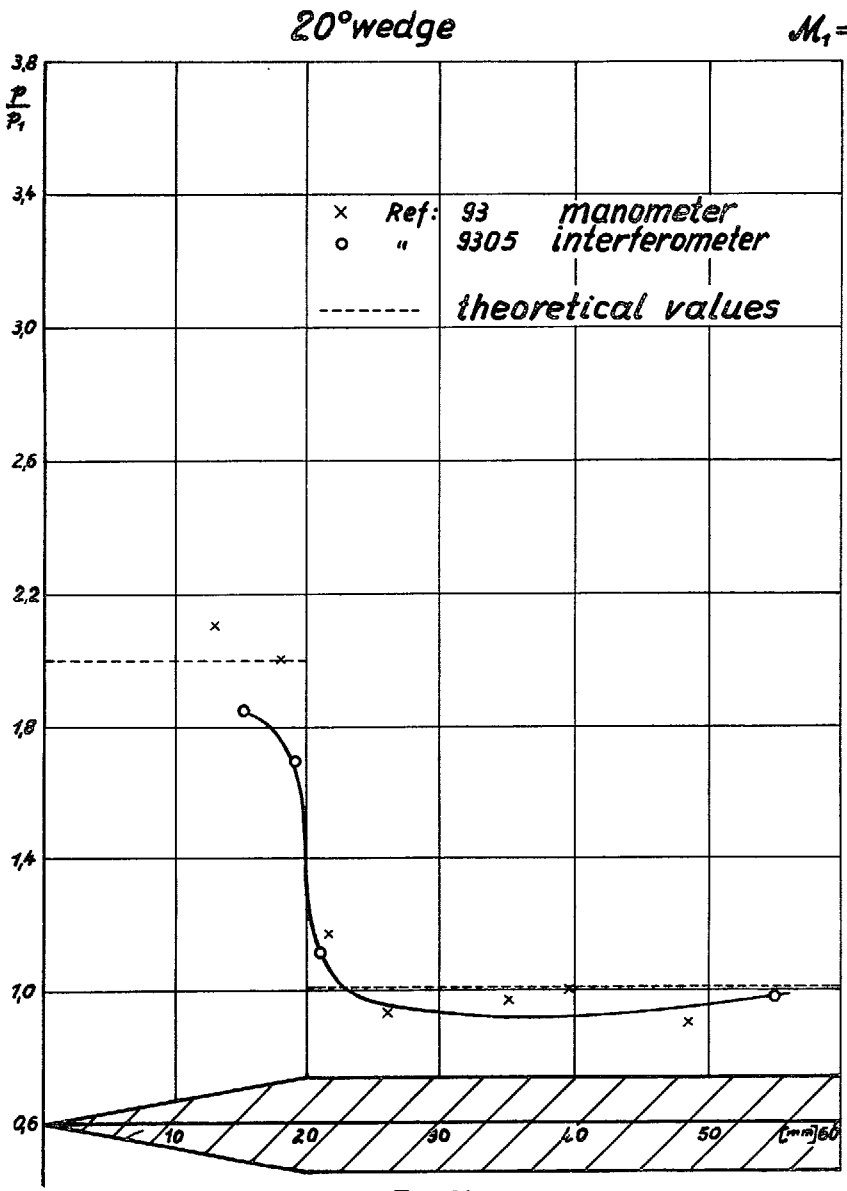

FIG. 20.

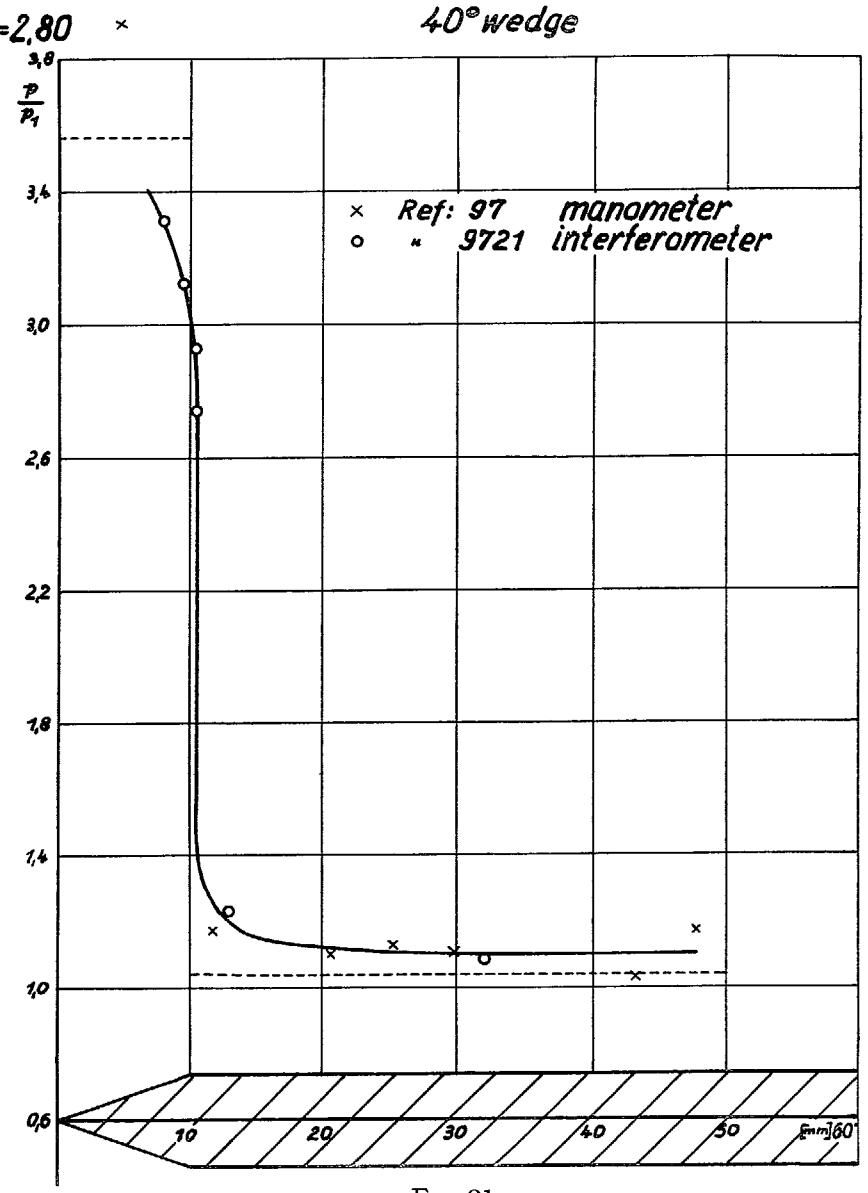

FIG. 21.

Pressure Distribution about the 20° and 40° Wedge at $M_1 = 2{\cdot}80$.

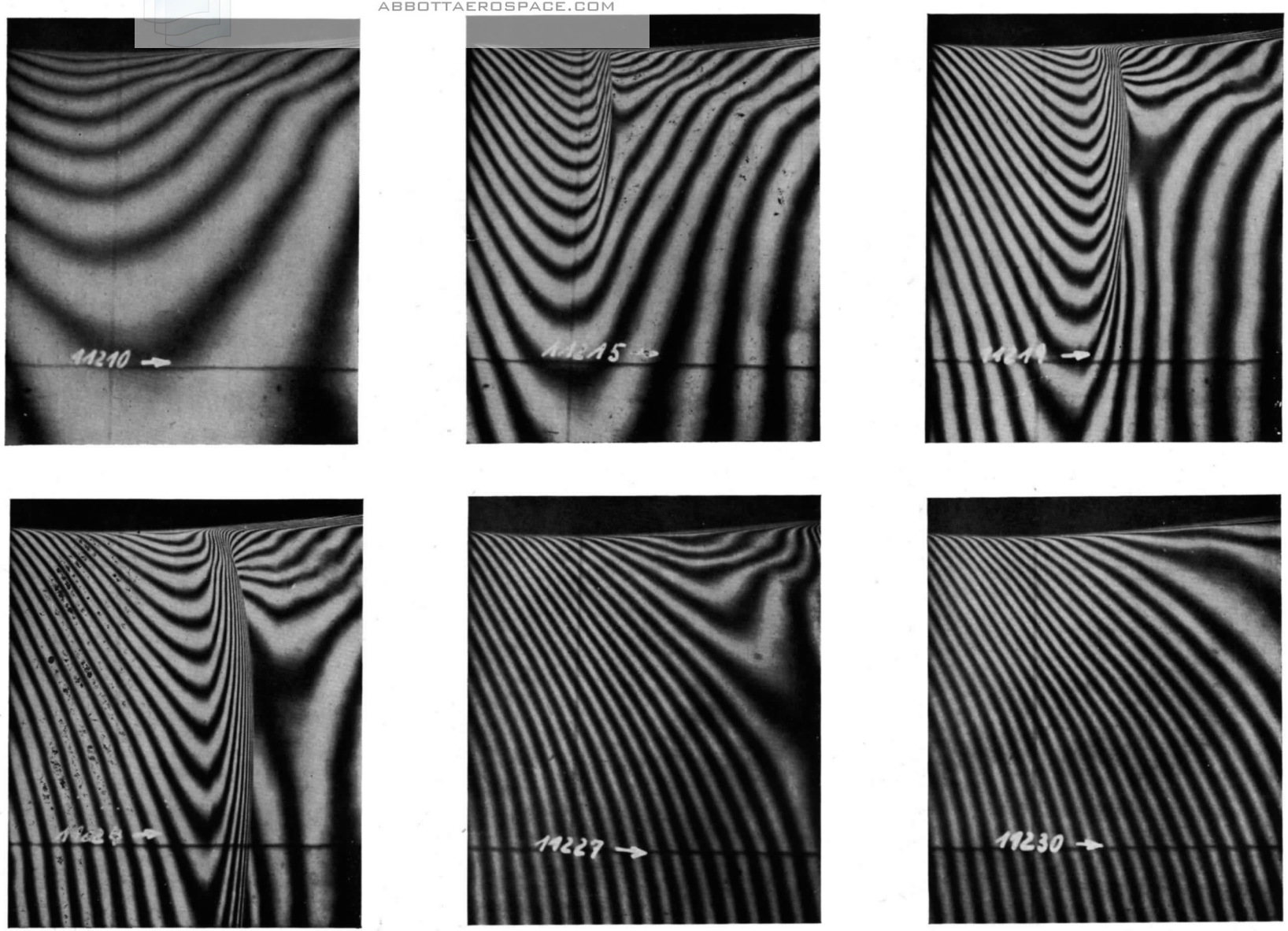

(Flow established).

FIG. 22. Throat Conditions in Empty ($M_1 = 1 \cdot 4$) Nozzle During Running-up of the Tunnel (density contour fringes).

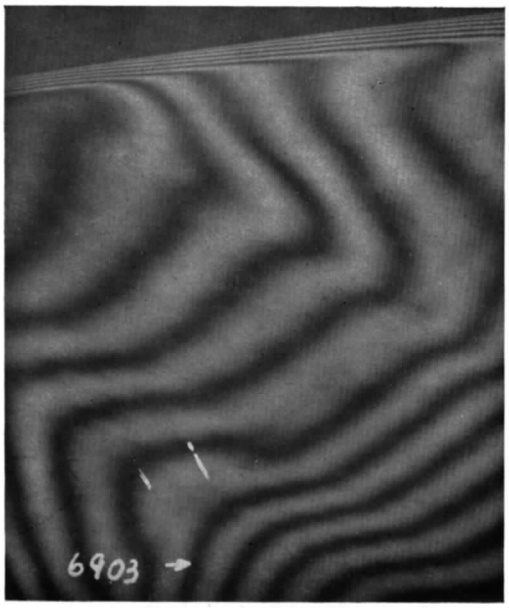

Near throat of $M_1 = 2{\cdot}0$ nozzle (Contour fringes).

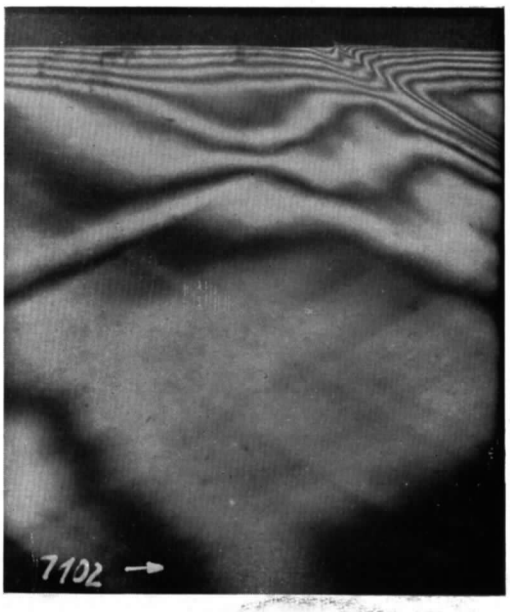

Flow at join of nozzle of $M_1 = 2{\cdot}0$ and wooden endpieces. (Contour fringes.)

Between throat and working-section of nozzle of $M_1 = 2{\cdot}8$. (Contour fringes.)

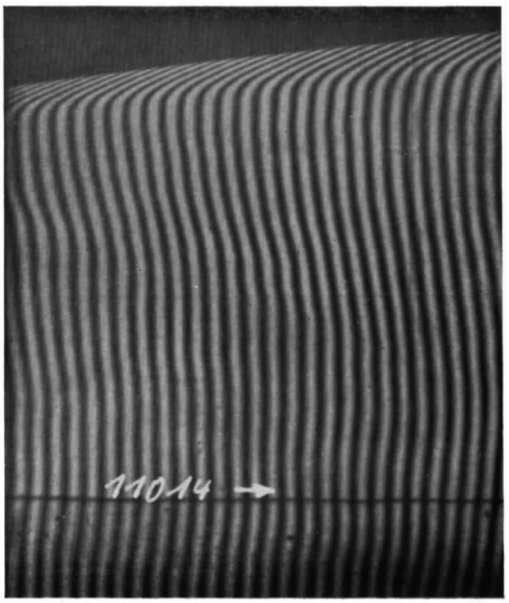

Between throat and working-section of nozzle of $M_1 = 2{\cdot}8$. (Displacement fringes.)

FIG. 23. Boundary-layer Photographs.

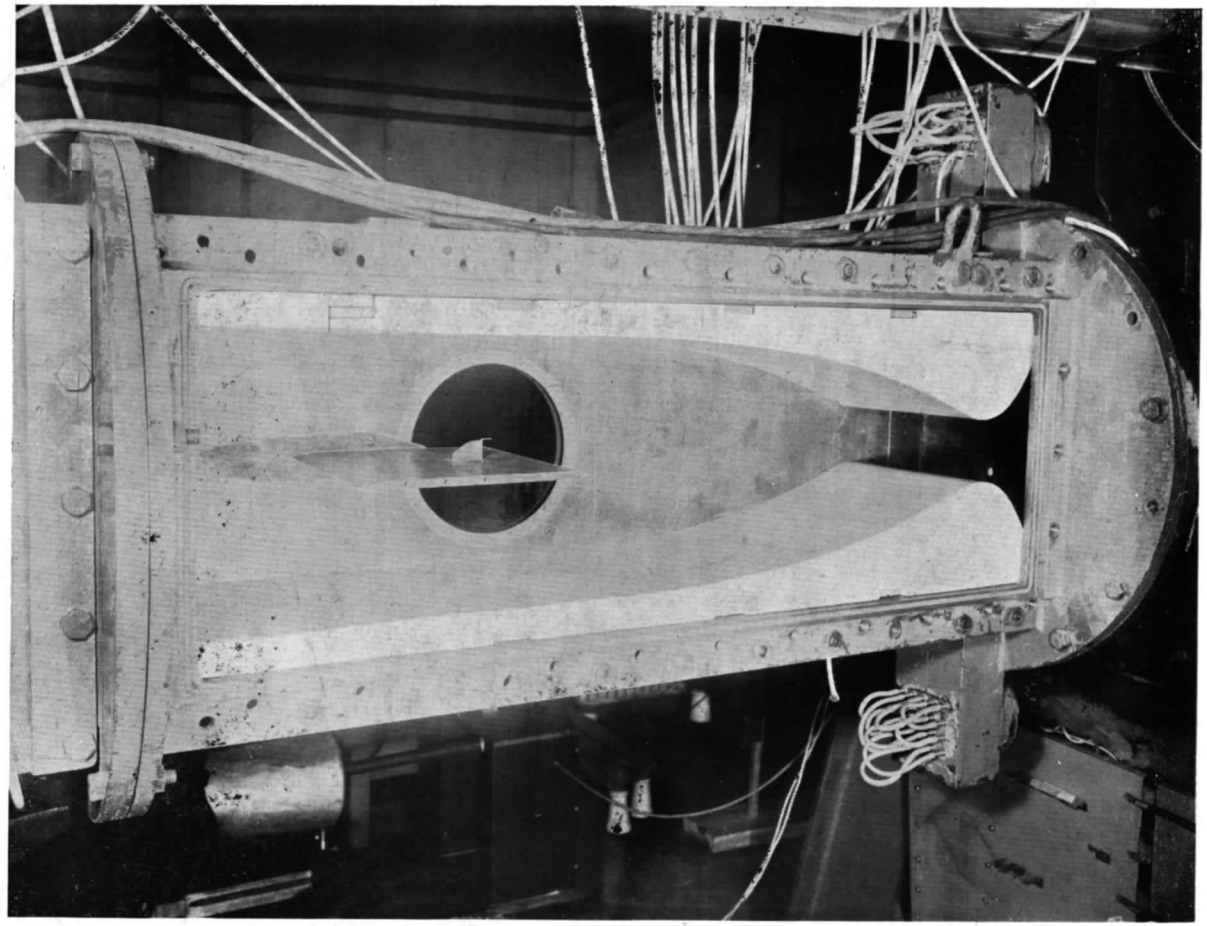

FIG. 24. 40° Wedge Installed in Tunnel with Nozzle for $M_1 = 2{\cdot}8$.

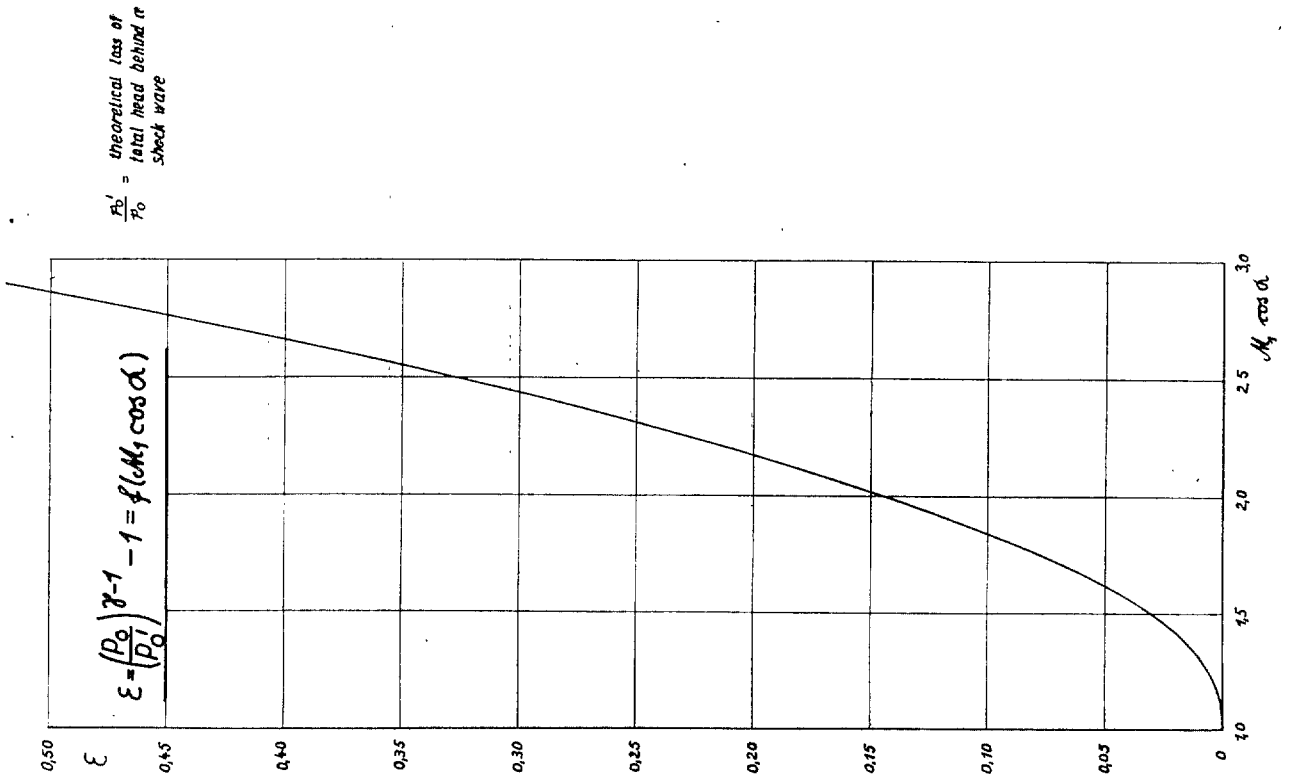

FIG. 26.

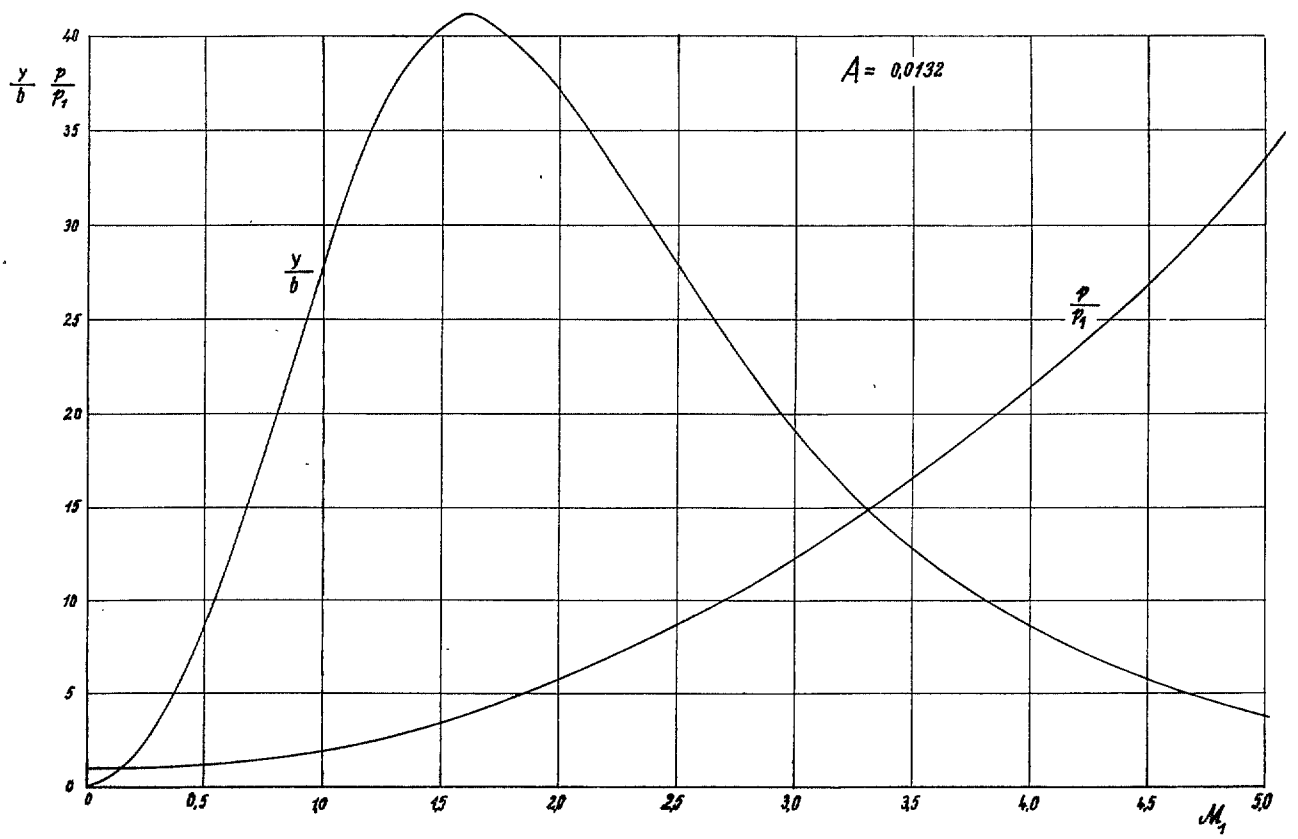

FIG. 27. Pressure Coefficient $\frac{p}{p_1}$ at the Stagnation Point and the Corresponding Fringe Shift $\frac{y}{b}$.

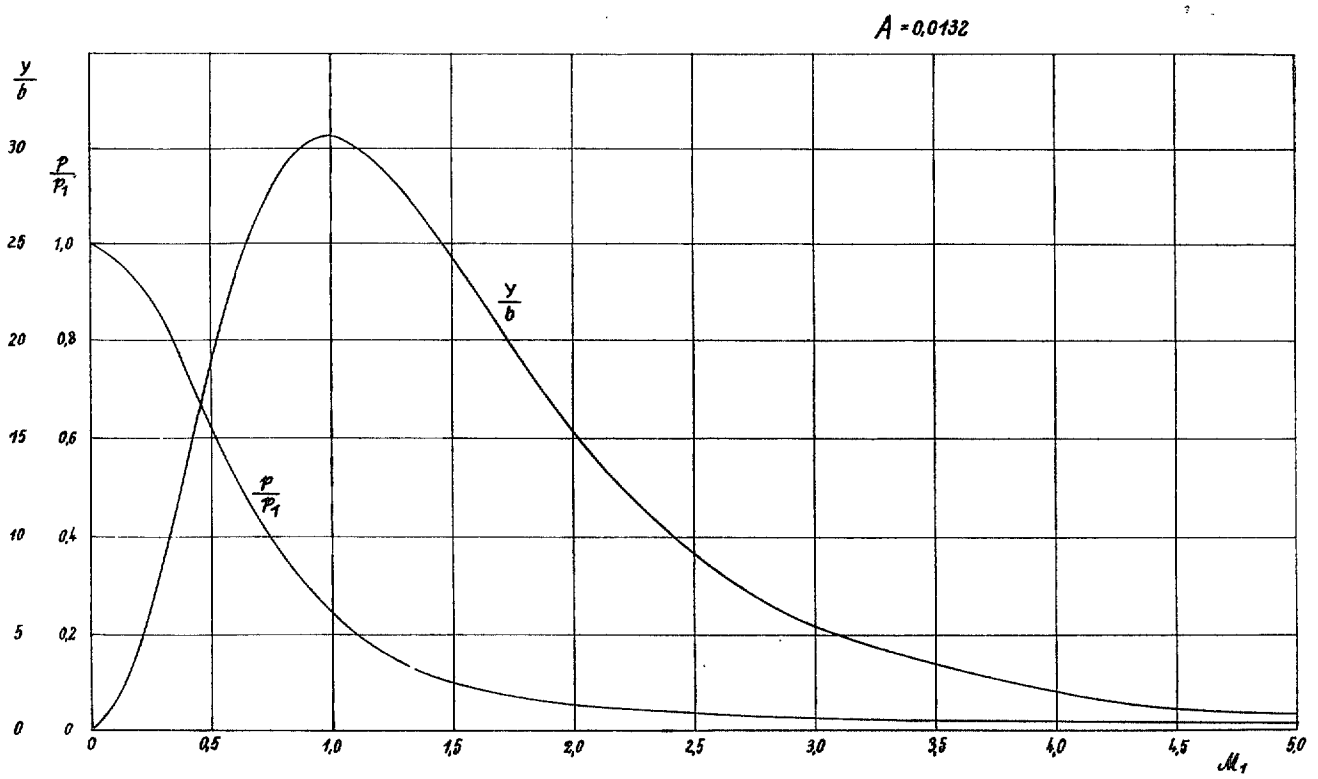

FIG. 28. Pressure Coefficient $\frac{p}{p_1}$ and Corresponding Fringe Shift $\frac{y}{b}$ at a Point where the Local Mach Number is Double that of the Undisturbed Flow.

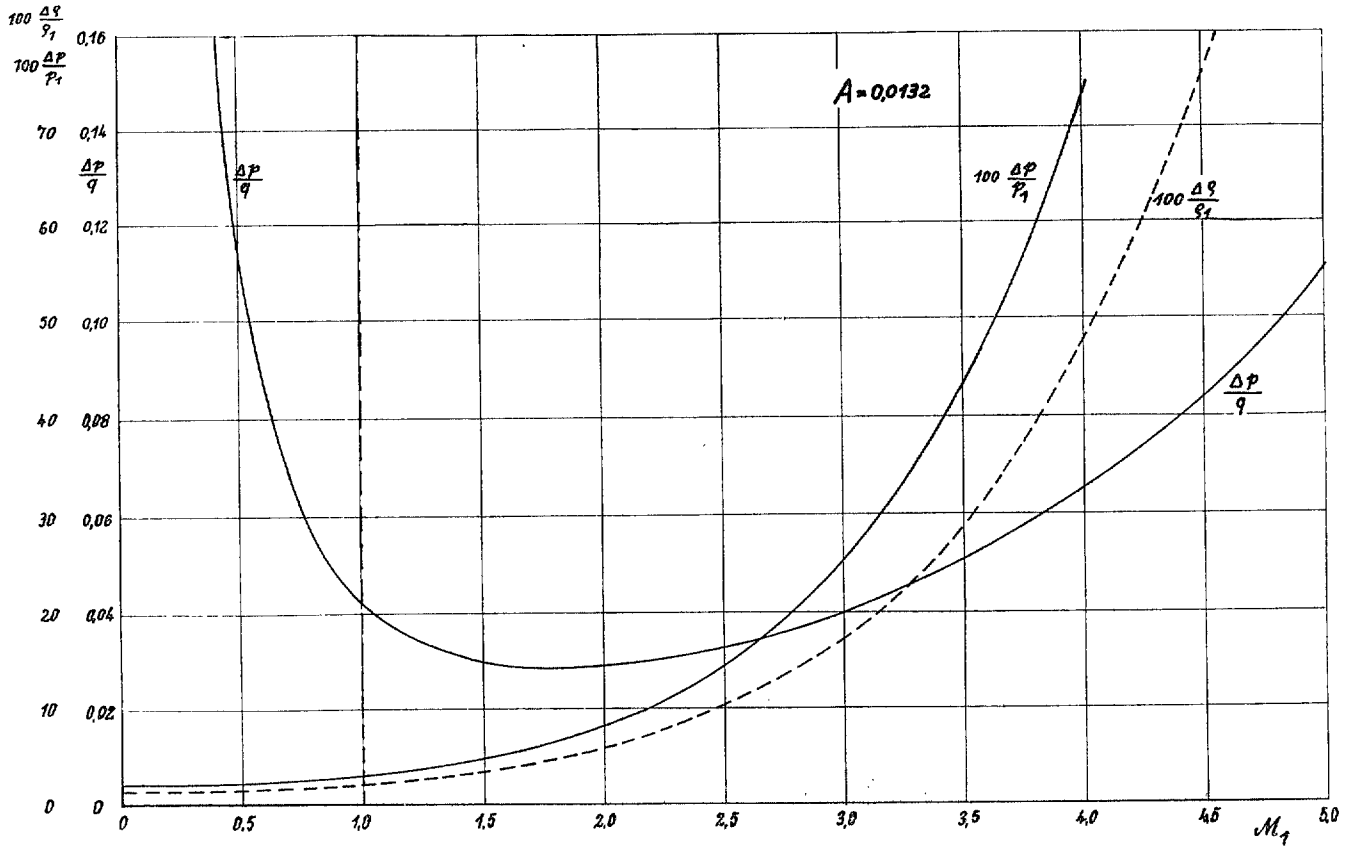

FIG. 29. Percentage Error in Density and Pressure, and the Error in the Pressure Coefficient $\frac{\Delta p}{q}$ for a Shift of One Fringe.

(87577) Wt. 12/818 K 5 11/49 Hw

PRINTED IN GREAT BRITAIN

R. & M. No. 2321
(10,462)
A.R.C. Technical Report

Publications of the Aeronautical Research Committee

TECHNICAL REPORTS OF THE AERONAUTICAL RESEARCH COMMITTEE—

1934–35 Vol. I. Aerodynamics. 40*s.* (40*s.* 8*d.*)
Vol. II. Seaplanes, Structures, Engines, Materials, etc. 40*s.* (40*s.* 8*d.*)

1935–36 Vol. I. Aerodynamics. 30*s.* (30*s.* 7*d.*)
Vol. II. Structures, Flutter, Engines, Seaplanes, etc. 30*s.* (30*s.* 7*d.*)

1936 Vol. I. Aerodynamics General, Performance, Airscrews, Flutter and Spinning. 40*s.* (40*s.* 9*d.*)
Vol. II. Stability and Control, Structures, Seaplanes, Engines, etc. 50*s.* (50*s.* 10*d.*)

1937 Vol. I. Aerodynamics General, Performance, Airscrews, Flutter and Spinning. 40*s.* (40*s.* 9*d.*)
Vol. II. Stability and Control, Structures, Seaplanes, Engines, etc. 60*s.* (61*s.*)

1938 Vol. I. Aerodynamics General, Performance, Airscrews, 50*s.* (51*s.*)
Vol. II. Stability and Control, Flutter, Structures, Seaplanes, Wind Tunnels, Materials. 30*s.* (30*s.* 9*d.*)

ANNUAL REPORTS OF THE AERONAUTICAL RESEARCH COMMITTEE—

1933–34 1*s.* 6*d.* (1*s.* 8*d.*)
1934–35 1*s.* 6*d.* (1*s.* 8*d.*)
April 1, 1935 to December 31, 1936. 4*s.* (4*s.* 4*d.*)
1937 2*s.* (2*s.* 2*d.*)
1938 1*s.* 6*d.* (1*s.* 8*d.*)

INDEXES TO THE TECHNICAL REPORTS OF THE ADVISORY COMMITTEE ON AERONAUTICS—

December 1, 1936 — June 30, 1939.	R. & M. No. 1850.	1*s.* 3*d.* (1*s.* 5*d.*)
July 1, 1939 — June 30, 1945.	R. & M. No. 1950.	1*s.* (1*s.* 2*d.*)
July 1, 1945 — June 30, 1946.	R. & M. No. 2050.	1*s.* (1*s.* 1*d.*)
July 1, 1946 — December 31, 1946.	R. & M. No. 2150.	1*s.* 3*d.* (1*s.* 4*d.*)
January 1, 1947 — June 30, 1947.	R. & M. No. 2250.	1*s.* 3*d.* (1*s.* 4*d.*)

Prices in brackets include postage.

Obtainable from

His Majesty's Stationery Office

London W.C.2 : York House, Kingsway
[Post Orders—P.O. Box No. 569, London, S.E.1.]

Edinburgh 2 : 13A Castle Street
Birmingham 3 : 2 Edmund Street
Bristol 1 : Tower Lane
Manchester 2 : 39 King Street
Cardiff : 1 St. Andrew's Crescent
Belfast : 80 Chichester Street

or through any bookseller.

S.O. Code No. 23-2321